March 2024

An Antiviral Response Unleashed: Deciphering the Relationship between Shiftless and RNA Granules during KSHV Infection

David C. Hatfield
University of Massachusetts Amherst

AN ANTIVIRAL RESPONSE UNLEASHED: DECIPHERING THE RELATIONSHIP BETWEEN SHIFTLESS AND RNA GRANULES DURING KSHV INFECTION

A Thesis Presented

by

DAVID C. HATFIELD

Submitted to the Graduate School of the University of Massachusetts Amherst in partial fulfillment of the requirements for the degree of

MASTER OF SCIENCE

February 2024

Microbiology Department

AN ANTIVIRAL RESPONSE UNLEASHED: DECIPHERING THE RELATIONSHIP BETWEEN SHIFTLESS AND RNA GRANULES DURING KSHV INFECTION

A Thesis Presented

by

DAVID C. HATFIELD

Approved as to style and content by:

_____

Mandy Muller, Chair

_____

M. Sloan Siegrist, Member

_____

Yasu S. Morita, Member

_____

James Holden, Department Head

Microbiology

ACKNOWLEDGMENTS

I would first like to extend my deepest gratitude to Dr. Mandy Muller for being the best research mentor that I could ask for. Thank you for not immediately deleting a random email from a guy in the Air Force. I will always appreciate that you accepted me into your lab even though I did not have traditional lab training/skills and during a time when the lab was already quite full. You have helped me whenever I needed it and pushed my goals further than I dared dream. The Muller lab has truly been a very encouraging and safe environment, where I could push the boundaries of science and not be afraid to fail. Thank you for everything!

I would like to next thank all the members of the Muller lab. Thank you Will (Dr. Rodriguez) for being a fantastic student mentor. You taught me so very much about experimentation, presentation, and how to be a driven worker who has joy in what he does. You have poured so much undeserved time and effort into me, of which I am so grateful for. Regarding the commitment to leadership and mentorship, you pushed the boundaries for what I thought these roles could assume, and this I hope to bring with me wherever I go in the future. Thank you to Jake, Yadi, Sam, and Dan for always being willing to drop whatever you are doing to help me and teach me. You all contributed so much to my education and growth as a human being this past year.

Next, I would like to thank the instructors and researchers in my scientific career who got me to where I am today. Thank you, Dr. Robert Langdon for truly being the most inspirational teacher that I have ever had. Your tutelage in biology not only inspired me to pursue the subject to a master's degree, but it also provided a solid foundation for all my coursework thus far. Your dedication to teaching and your faith in me has made an impact far greater than you will ever know. Thank you, Dr. Ragunath Chandran and Dr. John Cuozzo (both formerly of ZebiAI

Therapeutics) for giving me my first ever laboratory experience. During my internship, you taught me the foundational skills of research and showed me the fun of lab work. I am so grateful for the opportunity to have learned early in my professional career that work doesn't have to feel like work, and that I can enjoy what I do while making an impact. Thank you, Dr. Chia Hung and Dr. Jordan Steel for both teaching me so much during my time as an undergraduate at USAFA. You both believed in me and encouraged me to press on in times where it would have been very easy to coast and accomplish the minimum.

Penultimately, I would like to thank my family at Mercy House. During my time in Amherst, you have all loved, cared for, inspired, and changed me greatly. I enjoy working, sometimes maybe too much… You taught me how to have a work-life balance and the importance of putting my faith first. You showed me a Christ-centered perspective. God bless you all!

Lastly, I would like to thank my family. Kristin and Noah, you both teach me how to have fun in life and how to love others better. Thank you for giving me refuge at times when life becomes overwhelming. Mom and Dad, I love you both so much and would not be who I am today without your sacrifice, example, and copious amounts of blessings and grace. Thank you for supporting me and providing a home where I can flourish. Mom, thank you for teaching me how to do 'useful things', stay organized, and work harder than I did yesterday. Dad, thank you for teaching me patience, persistence, and the perspective to never 'wish your days away.' To my Molly, I am so very grateful to have fallen insanely in love with you. Thank you for keeping me grounded and blessing me abundantly. I am so thankful for this season and to spend the rest of my life with you. I love you all.

ABSTRACT

AN ANTIVIRAL RESPONSE UNLEASHED: DECIPHERING THE RELATIONSHIP BETWEEN SHIFTLESS AND RNA GRANULES DURING KSHV INFECTION

FEBRUARY 2024

DAVID C. HATFIELD, B.Sc., UNITED STATES AIR FORCE ACADEMY

M.S., UNIVERSITY OF MASSACHUSETTS AMHERST

Directed by: Professor Mandy Muller

Herpesviruses persist as a parasitic actor among many species. These viral agents can rapidly seize control over host cells by influencing global gene expression. Through a process known as host shutoff, herpesviruses cause a widespread degradation event of host transcripts within the cytoplasm. Specifically, Kaposi Sarcoma associated herpesvirus (KSHV) encodes for an endoribonuclease, termed SOX, that orchestrates this manipulation of gene expression. We and others have discovered certain transcripts that escape this fate; we suggest that this is an active escape, where transcripts have 3' UTR elements that disallow SOX cleavage. One of the escapees that has been found is that of C19ORF66, which encodes the protein known as Shiftless (SHFL). SHFL is a broadly characterized antiviral host factor that may also be stimulated via interferons. Through our investigation of SHFL during KSHV infection, we have also observed this host factor acting in opposition to viral agents. We have also uncovered that SHFL

expression causes the loss of P-bodies, a constitutively present RNA granule. We postulate that SHFL ability to regulate P-bodies directly contributes towards its antiviral capacity and serves as a rare example of host-P-body regulation. Through further characterization of this pro-host factor, we hope to provide a deeper understanding of subcellular mechanisms and host gene expression during KSHV infection.

TABLE OF CONTENTS

Page

LIST OF TABLES

LIST OF FIGURES

Figure.....Page

INTRODUCTION

1.1 Kaposi's Sarcoma associated Herpesvirus (KSHV)

Herpesviruses are evolutionarily robust parasites. Following entry into the host, their bi-phasic lifecycle promotes a lifelong infection and a nearly global distribution of virus among humans. Established after primary infection of select cell types, latency preserves the viral genome as extra-chromosomal episomes within the nucleus, allowing for carefully regulated and minimal viral gene expression to avoid immune sensing. However, when the host cell is faced with environmentally unfavorable stimuli, herpesviruses will "reactivate" back into a state of active lytic replication allowing for efficient virion production and dissemination to new hosts. Kaposi Sarcoma Associated Herpesvirus (KSHV) is an oncogenic gammaherpesvirus and is one of the leading causes of cancer among immunocompromised individuals such as HIV-AIDS patients and organ transplant recipients [1]. KSHV is the causative agent of its namesake disease Kaposi Sarcoma (KS), an epithelial cell skin cancer, multicentric Castleman's disease (MCD) and primary effusion lymphoma (PEL) [1, 3, 4, 142, 143].

KSHV is a double stranded DNA virus with a genome roughly 165kB in size [144]. KSHV establishes itself within much of the population, sidestepping immunocompetency, through a lifelong latent infection. During this phase, the virus maintains its genome on extrachromosomal episomes within the nucleus of a host, where mitosis leads to the replication of the host genome alongside these circular, viral DNA molecules [1]. Daughter cells thus inherit a copy of the viral genome, perpetuating latency and leading to viral persistence. To maintain this passive existence, KSHV must also take the form of viral particles that can spread to neighboring cells; otherwise, the virus could risk its survival. Following latency, KSHV enters a more active phase: lytic reactivation. In particular, KSHV's replication and transcription

activator (RTA) has been implicated as the central element of this switch in gene expression from latent to lytic genes [2]. RTA has been shown to influence its own promoter as well as the expression of lytic genes such as polyadenylated nuclear (PAN) RNA, ORF57, K14, ORF74, and K9 [3-6, 2, 7-9]. Factors such as oxidative stress, hypoxia, cell signaling, and co-viral infection can all contribute to the induction of KSHV reactivation [10]**.** Ultimately, this lytic reactivation enables the virus to efficiently hijack the host for virion production and transmission to new hosts.

1.2 Viral Host Shutoff

Surprisingly, several gammaherpesviruses including KSHV, Epstein-Barr virus (EBV), Murine Herpesvirus 68 (MHV68), and the alphaherpesvirus Herpes Simplex Virus-1 (HSV-1) have all converged on the same strategy for rapidly seizing control of cellular gene expression during lytic replication, namely viral host shutoff. Viral host shutoff involves a global RNA decay event where the vast majority of cellular mRNA are degraded following viral infection; gammaherpesviral endoribonucleases help induce this RNA turnover [11-14]. This cellular process simultaneously mutes host gene expression and liberates critical cellular gene expression resources for viral gene expression [15-17]. Several studies emphasize the importance of host shutoff as critical strategy to successful infection, where loss of this phenotype cripples herpesviral replication [18, 19]. For KSHV, like many of the herpesviruses, host shutoff is orchestrated from the cytoplasm by a single viral protein, the viral endoribonuclease SOX (encoded by ORF37). SOX expression alone, even outside the context of infection, induces the degradation of greater than 70% of the cellular transcriptome [20, 21]. However, despite the magnitude of SOX induced host shutoff, not all transcripts meet this fate, as a remaining roughly 30% of mRNAs escape SOX cleavage [20, 21]. Certain transcripts have been characterized as

"passive" escapees, meaning that they simply lack the necessary SOX targeting motif(s) to prime the viral endoribonuclease for cleavage [22]. Fascinatingly, there are also mRNA that actively evade SOX cleavage via a secondary structure mapped to 3' untranslated regions (UTR) termed the "Sox resistant element" or SRE [23-28]. By 2019, there were two known SRE-bearing escapees including the host interleukin-6 (IL-6) [20, 26, 28] growth arrest and DNA damage inducible 45 beta (GADD45B) mRNA [22]. As such, to better understand this escape phenotype, our lab previously set out to expand our list of known escapees. Thus, using an unbiased RNA-seq approach and subsequent hierarchal clustering, we identified a list of 75 transcripts that are capable of escaping multiple herpesviral endoribonucleases [21]. From this list, we validated the escape of several mRNA that demonstrated the greatest capacity for evading cleavage (**Figure 1**) [21]. From this screen, we identified a third SRE-bearing transcript: C19ORF66 (recently renamed Shiftless [29]) [21]. Excitingly, the SHFL SRE also confers a striking resistance to the Influenza A virus PA-X endonuclease [21]. This significant breadth of resistance to cleavage by such a broad diversity of host shutoff proteins highlights the evolutionary imperative for the expression of SHFL during viral infection.

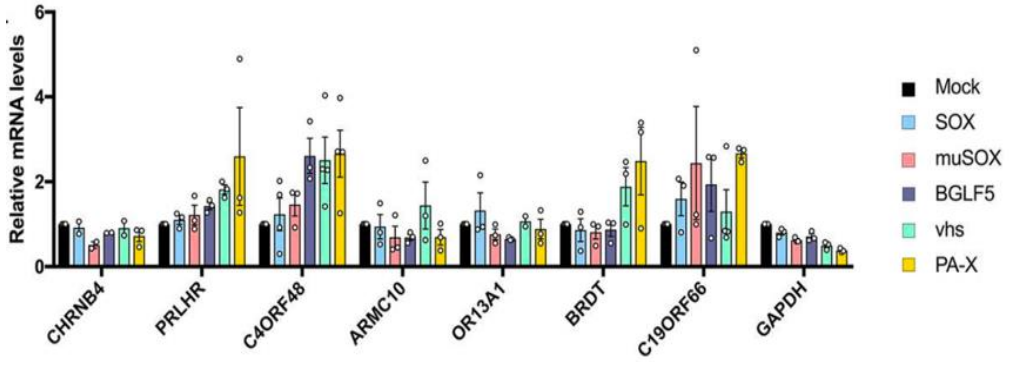

Figure 1: Top escapees' mRNA levels following viral endonuclease activity. These potential candidates were identified by RNA-seq data following KSHV lytic reactivation. Plasmids expressing the escapees and the indicated endonucleases were expressed in HEK293T cells for 24 h. Total RNA was harvested and relative mRNA abundance for these candidates. [21]

1.3 The Structure and Function of Shiftless (SHFL)

In 2016, Shiftless was first identified and reported as a bona-fide interferon-stimulated gene (ISG), whose expression is tightly regulated by Type I, Type II, and Type III interferon [30-37]. Since these initial studies, SHFL has been found to be a potent anti-viral factor, restricting multiple DNA, RNA, and Retroviruses including the recent pandemic associated coronavirus SARS-CoV-2 [38, 30, 31, 39, 32, 33, 40, 34, 41, 42, 21, 43, 44, 35, 29, 45, 36, 46, 37]. The appearance of the SHFL transcript in pulldowns during KSHV lytic replication proved to be a very exciting host defense prospect because of some of the anti-viral roles that this protein has in the context of other viral infection models.

The SHFL gene is located on chromosome 19 (NC_000019.10), encodes for eight exons which yield four isoforms. The full length SHFL isoform, C19ORF66-201, is 1928nt long and encodes for a 291aa protein. This 33kDa protein has been predicted to have eight α-helices, seven β-sheets, a zinc ribbon motif (aa 112-135), a nuclear localization signal (NLS) (aa 121-173), a coiled-coil motif (aa 261–285), a nuclear export signal (NES) (aa 261-269), and a glutamic acid rich region in the C-terminus **(Figure 2A)** [53]. Each of the SHFL isoforms maintain a strict cytoplasmic localization with the peculiar exception of C19ORF66-209, which lacks the canonical C-terminal NES, but does not demonstrate anti-viral function [29]. Given the lack of a crystal structure and no clear enzymatic function, the anti-viral functions of SHFL are often attributed to cooperativity with other cytoplasmic RNA-binding proteins (RBPs) [54-56, 42]. Critical to these interactions are two functional domains of SHFL: the PABPC binding domain (aa 102-150) and the -1 Programmed Ribosomal Frameshift (-1PRF) effector domain (aa 164-199) **(Figure 2A)**. Of these two domains, most of SHFL anti-viral functions have been attributed to the PABPC-binding domain. As per its namesake, this domain coordinates a critical

interaction between SHFL and Poly-A Binding Protein Cytoplasmic 1 (PABPC1). PABPC1 is nucleocytoplasmic shuttling RBP that helps coordinate mRNA nuclear export and subcellular localization [57]. Due to its nearly universal RNA binding capacity, it has been shown to be critical for mRNA stability, localization, translation initiation, and elongation [58-63, 57, 64]. It has been demonstrated that interactions with PABPC1 and likely other RBPs enhance SHFL ability to bind to target mRNAs [38, 65, 42, 43]. In the context of DENV and several members of Flaviviridae, the interaction between SHFL and PABPC1 appears to be vital toward the capacity of SHFL to restrict RNA virus replication [66, 65, 43]. In accordance with these findings, further highlighting the importance of the PABPC-binding domain, recent work by Napthine and colleagues idnetified three arginie residues (R131, R133, R136) which have been shown to be critical for SHFL RNA binding *in-vitro* [41]. Notably, the group remarks that cofactors, such as PABPC or LARP1, likely still contribute to SHFL-RNA interactions in conjunction with these specific residues.

Alongside these domains, though not fully characterized , the C-terminal domain, which also contains the NES, is predicted to be a lone α-helix that may be neccesary for the previously hyptohesized dimerization of SHFL **(Figure 2B)** [53]. This potential of self-dimerization has been previously posited to be involved in SHFL capacity to regulate the -1 frameshift [53]. This homodimerization may also permit SHFL to influence its own regulation or alter affinities with interactors that could impact RNA stability or translation, as this is observed with other factors [67-69, 53, 70]. Given the diverse range of anti-viral mechnasism and the ambiguoius nature of the moleuclar functions of SHFL, further investigation of the domain arhcitecture and neccessity will be invaluable toward understanding its borader evoluitionary role duirng viral infection.

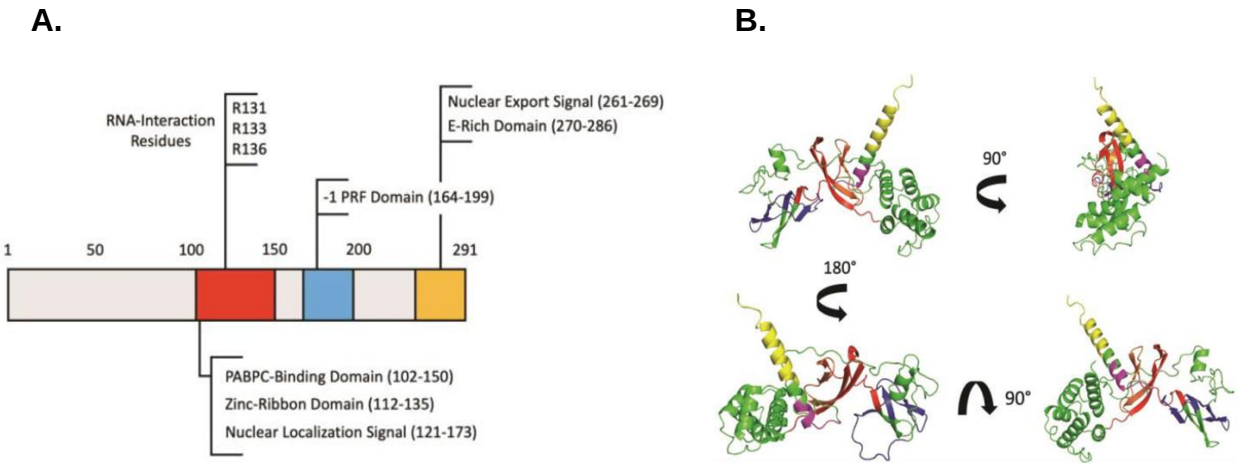

Figure 2: SHFL protein structure and characterized domains. **(A).** SHFL is 291aa long and ~33 kDa in molecular weight. Highlighted in red is the proposed PABPC/RNA binding domain, in blue the -1PRF domain that is responsible for SHFL namesake, and in yellow is the C-terminal, glutamic acid rich domain that is highly influential over SHFL localization. **(B).** Alphafold2 Structural Prediction for SHFL. The previously mentioned domains can be seen again here in red, blue, and yellow. In pink, the SHFL nuclear export signal is highlighted. [53]

One of the most interesting facets of SHFL is that for nearly every virus SHFL has been shown to restrict, a novel molecular mechanism of action has been described **(Figure 3)**. First, the SHFL -1PRF doamin (aa163-199) has been observed to have an interesting impact on viral transcription for HIV-1, WNV, JEV, and select coronaviruses like SARS-CoV2 [47-50]. These viruses take advantage of the host ribosome that can slip or shift position on actively translating mRNAs within the cytoplasm. The -1 programmed ribosomal frameshift is a translation based strategy for recoding; this can actively allow for one mRNA molecule to encode for more than one polypeptide chain. The -1PRF singal consists of two motifs: a heptameric slippery sequence and an RNA pseudoknot downstream of the slippery sequence. Slippery sequences are elements that initiate frameshifting, while structural elements like psuedoknots contribute to the efficiency of this slippage [145]. The combination of these motifs on an mRNA causes the translating ribosome to shift frame backwards by one nucleotide. Starting in a 0 frame and shifting to a -1

frame alters every downstream codon. For viruses, maintianing a small genome that efficiently enocdes for critical proteins will best promote viral evasion from host immune sensors and ensure virion production. Previous work has identified that HIV-1 utilizes a -1PRF to alter the ratio of Gag and Gag-Pol polyproteins [51]. The importance of this structural protein and reverse transcriptase cannot be overstated, for without either, HIV-1 would not plague the world as it does. Yet, both of these essential proteins are subject to -1PRF control. In an effort to identify host factors that may be involved in the HIV-1 -1PRF translation strategy, proteomic screenings revealed SHFL as a ribosomal interactor [29]. These findings ultimately resulted in C19ORF66 acquiring the name "Shiftless" (SHFL) because it was observed to supress this ribosomal frameshift in the context of HIV-1 infection as well as several other retroviruses (RSV, MMTV, HTLV, HIV-2, and SIV) [29]. It has been proposed that SHFL binds to mRNAs with -1PRF motifs in response to the ribosome stalling at said regions [29]. Instead of allowing time for the ribosomal complex to contort and rotate (and ultimately lead to the frameshift), SHFL in unison with factors such as Eukaryotic polypeptide chain release factor 3 (eRF3) and eRF1 bind to the stalled ribosome and prematurely terminate translation [52]. Thus, SHFL can impact viral translation by preventing ribosomal reading of mRNAs in multiple frames.

Second, it has been demonstrated that interactions with PABPC1 and other RBPs enhance SHFL ability to bind to target mRNA [43]. In the context of DENV infection, SHFL has been shown to be a critical piece of the host immune response. SHFL expression led to viral restriction, while knockdown of the protein caused host immune effectiveness to wildly decrease [43]. Independently, RBPs, such as PABPC1 are thought to act in a pro-viral way. However, given these SHFL results during DENV infection and SHFL known interaction with PABPC1, it has been proposed that the ISG somehow repurposes PABPC1 or at the very least mutes its pro-

viral effects [53]. Other groups have identified that SHFL has an affinity for viral RNA in the context of HCV and YFV replication and can also restrict both agents [39]. SHFL ability to bind to viral RNA via the 49aa domain (aa 102-150) **(Figure 2A)** may indicate that these transcripts are being tagged and targeted for degradation or their localization and accessibility are being altered through cytoplasmic condensates, such as Processing Bodies (P-bodies) or Stress Granules (SGs) [38]. This central domain of SHFL, responsible for the interaction with PABPC1 and contributory for RNA binding, has been thoroughly observed to be active and relevant during the context of viral infection [43, 53, 65]. Third, it has been observed that in the context of yellow fever virus (YFV) and hepatitis C virus (HCV) that SHFL disrupts viral RNA replication [40, 53]. Through electron microscopy, SHFL has been observed to alter the HCV replication network, often referred to the viral membranous web [40]. Fourth, SHFL has been seen to facilitate the degradation of viral proteins [45, 46, 53]. This degradation functionality has been observed to contribute to lysosomal pathways as well as ubiquitylation/proteasomal pathways. These functions likely feed SHFL ultimate functionality as an ISG: prevent and mitigate host devastation orchestrated by parasitic invaders. Though some domains of SHFL have been explored, more remains to be characterized about this protein and how it specifically plays a role during viral infection. Thus, as an escapee of viral endoribonuclease induced host shutoff, SHFL presented itself as a fascinating candidate for study particularly during KSHV lytic replication.

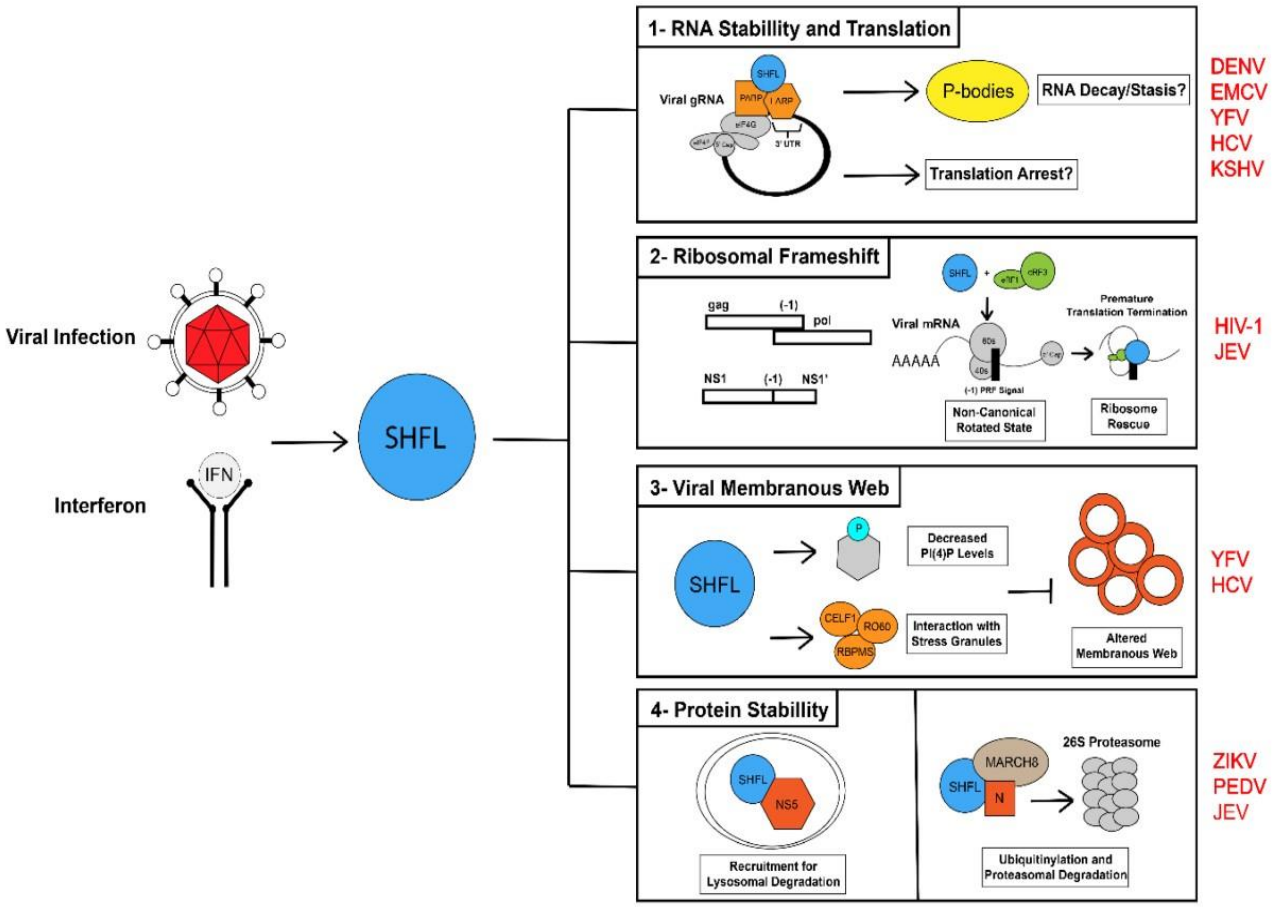

Figure 3: SHFL antiviral functions and mechanisms. **1.** SHFL impacts viral RNA stability and translation. Specifically, with flaviviruses SHFL binds to viral RNA causing translational arrest, which may be achieved by transcript re-localization to P-bodies. **2.** SHFL helps to identify frameshifting and cause ribosomal release from viral transcripts. **3.** This antiviral factor has been shown to decrease PI(4)P levels which can serves as a critical component of certain viral replication networks. **4.** SHFL has also been implicated as a facilitator for certain viral protein degradation pathways, to include ubiquitination and lysosomal degradation. [53]

1.4 RNA Granules

Biomolecular condensates, fundamentally, are densities of specific molecular material that are grouped for a subcellular organization purposes [71]. Over recent decades, condensates have gained increasing attention; at the beginning stages of their characterization, high resolution microscopy revealed foci that could rapidly exchange material with their surroundings in seconds to minutes [72-74]. Some biomolecular condensates are constitutively present, while others

require some method of induction [75, 76]. Densities of biomolecules, including RNA and protein, can allow for cells to combat cellular overcrowding and may contribute to energetic conservation. Condensates also provide a more dynamic solution for the regulation of certain processes by eliminating the separation of two states by a phasic physical barrier. Depending upon location, conditions, and necessity, condensates can either sequester molecules for inhibitory purposes or enhance local density to increase reactivity and interaction [71]. Thermodynamically, within a complex system of solvent and solutes, relative affinities dictate many interactions [77]. Phase separation can primarily be determined by modulator concentration alongside influential conditions, such as pH, temperature, pressure, and environmental factors [77]. Biomolecular foci do not have the phospholipid bilayers that eukaryotic organelles possess to distinctly define spatial and molecular boundaries. Often condensates are referred to as being Liquid-Liquid phase separated (LLPS); however, to quickly characterize these foci as such would be an oversimplification. LLPS paints a generic picture of two simple, non-mixing, and viscous liquids [78]. *In vivo*, the process remains more complex; these granules are better described as viscoelastic networks containing diverse sets of macromolecules with dynamic interactions [78]. Viscoelasticity may be defined as a network of structural components and moduli that are both viscous and elastic, broadly time-dependent upon stress-strain relationships [78]. Using LLPS as a classification system for condensates can be a helpful mental image for this hard-to-grasp dynamic subcellular organization strategy. However, one must be careful to not overlook the complex nature of theses densities and how they beautifully form at a microscopic level while being subject to so many conditions that must be ideal for formation to exist. Notable cytoplasmic granule examples include Processing Bodies (P-bodies), Stress granules (SGs), Balbiani bodies, Germ granules, U-bodies, and RNA transport

granules [71]. Nucleoplasmic granule types are PcG bodies, Paraspeckles, Cajal bodies, PML bodies, DNA damage foci, cleavage bodies, and many more [71]. These categorizations of condensates within cells are not exhaustive nor are they always necessarily highly specific. Some of these granule types are broader groupings and not highly specific to exactly one density type. This caveat is not meant to discredit or discourage research into granules, but rather to reflect on the complexity of this developing field of subcellular organization that lack traditional definition. We hope to inspire more research into this area that still has many unexplored avenues. A broad diversity in biomolecular condensates naturally means a broad diversity in the functions of said densities; notably, transcript modification, RNA regulation, and modulation of translation exist as functional outputs for many condensates [79, 80, 75, 76, 81]. Many of these condensates impact both translation and gene expression in manners of promotion or suppression. P-bodies are dense RNP foci that are constitutively present in the cytoplasm of several cell lines [146]. Several conserved protein components of P-bodies include but are not limited to: DCP1, DCP2, Xrn1, EDC3, hedls/EDC4, and DDX6 [82, 83, 76, 84]. These constituents often lead to P-bodies being classified as sites of mRNA decay, especially in the early stages of characterization [147, 148]. However, further analysis indicates that P-bodies are likely more broadly densities for RNA triage or storage since transcripts have been observed leaving P-bodies to re-enter the translation pool [85]. In fact, this RNA granule is not required for micro-RNA induced silencing or RNA decay [86, 87]. P-bodies are quite dynamic, where proteins alongside mRNAs can be seen to shuttle in and out of these organizational densities [76]. Though their regulation is not thoroughly understood, P-bodies appear to be linked to polysomes and translation [88, 89]. Translation inhibitory agents, such as cycloheximide, have been observed to cause a loss of P-bodies [82]. Cycloheximide prevents the elongation of actively forming polypeptide chains and

leads to these stalled preinitiation sites of messenger ribonucleoprotein complexes (mRNP) to conglomerate in polysomes. Cycloheximide reduces the amount of readily available mRNP within the cytoplasmic system; this constriction of complexes to be incorporated into P-bodies has been suggested to be the cause of the foci loss [82, 76]. Oxidative stressors, such as sodium arsenite (NaAs) have been observed to induce P-body formation [90]. It has been suggested that NaAs stimulates distinct signaling pathways that are critical for P-body formation [89, 90].

1.5 Deciphering the Role of SHFL during KSHV Infection

1.5.1. Shiftless broadly restricts KSHV Lytic

After observing SHFL ability to persist during KSHV lytic replication, we in the Muller lab chose to evaluate this broadly acting, antiviral host factor thinking it could help us better understand the subcellular environment during herpesviral infection. Thus, we sought to determine the impact of SHFL expression on KSHV lytic replication following its escape from host shutoff to further understand the pro- or antiviral nature of the escape phenotype. To this end, through a series of overexpression and knockdown experiments within KSHV-positive iSLK.219 endothelial cell line [21], we found that SHFL stringently restricts KSHV lytic reactivation from latency and nearly every step of lytic replication thereafter **(Figure 4)** [21]. During lytic reactivation, gene expression of KSHV exists as a temporal cascade, where “early” (E) genes are expressed, followed by “delayed early” (DE), and then “late” (L) [21]. Upon further investigation, knockdown of SHFL and subsequent RT-qPCR analysis revealed this restriction was due to a clear impact of SHFL on early (ORF57) and delayed gene (ORF37) expression **(Figure 5)**. Interestingly, SHFL does not impact the expression of the late gene K8.1 suggesting that SHFL likely does not directly interfere with viral DNA replication [21]. These

results taken together demonstrate that following its escape from KSHV host shutoff, SHFL restricts KSHV lytic replication by impeding viral gene expression.

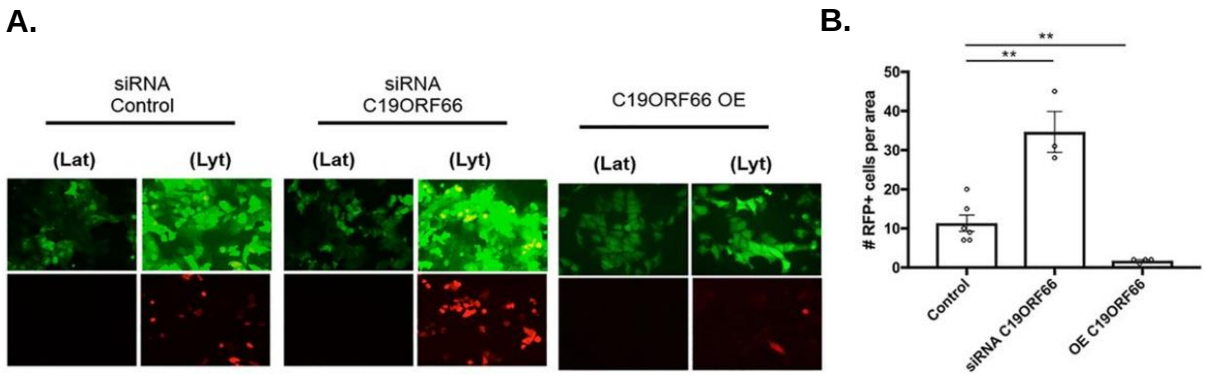

Figure 4: SHFL (C19ORF66) restricts KSHV lytic reactivation. **(A).** Knockdown and over-expression of SHFL identifies anti-KSHV factor. iSLK.219 cells were either treated with siSHFL or transfected with F-SHFL. Following 72 h of reactivation, fluorescence was captured via confocal microscopy. **(B).** Quantification of RFP cells for F-SHFL KD and over-expression. Randomized views were captured for the three conditions and RFP expression (reactivated cells) was quantified. [21]

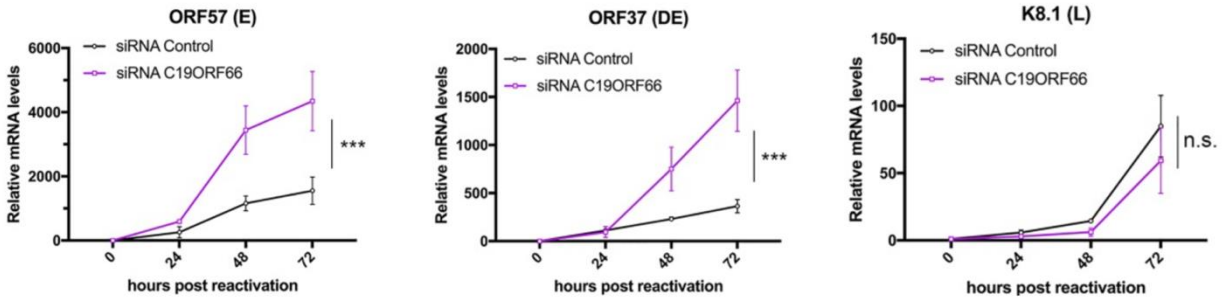

Figure 5: KSHV lytic gene expression under siSHFL. iSLK.219 cells were treated for 48 h with siSHFL or an siRNA control with no specific target. At the indicated time points, cells were harvested and subjected to RT-qPCR for analysis of the indicated genes. ORF57, ORF37, and K8.1 relative RNA levels represent the three categories for KSHV lytic genes: Early, Delayed Early, and Late. [21]

1.5.2. Deciphering the SHFL restriction Mechanism during KSHV Infection

Given the profound impact of SHFL on KSHV infection and its breadth of anti-viral activity against so many different RNA and retroviruses, we next sought to determine the molecular mechanism(s) by which SHFL restricts viral gene expression in the context of DNA virus infection. Given SHFL diverse characterization and broad array of viral restriction mechanisms we wanted to better understand what factors this protein may interact with. Therefore, we next mapped the SHFL interactome across KSHV infection (latent and lytic replication) using liquid chromatography-tandem mass spectrometry (LC-MS) [42]. LC-MS and protein interactomes help to identify a broader classification of protein-protein interactions. This interactome can help to characterize SHFL functionality by implicating this protein with either specific factors or with a large class of proteins that all carry out a similar function. LC-MS revealed 98 interactors of both viral and host origin. Through Gene Ontology (GO) term analysis, we found enrichment of proteins in functional categories that corroborated previously described functions of SHFL including: ubiquitin ligase binding [42], and importantly several RNA binding proteins. Among these RBP interactors included known SHFL interactor PABPC1 and several novel interactors: KPNA2, DDX3X, FUS, and HNRNPK. Of note, all these proteins are known constituents of cytoplasmic RNA granules, such as P-bodies or stress granules **(Figure 6)** [91, 92, 42, 93, 94]. Based on these observations, we became keenly interested in the relationship between SHFL and RNA granules, especially given their previously observed interplay in the context of RNA virus infection as aforementioned in the previous section.

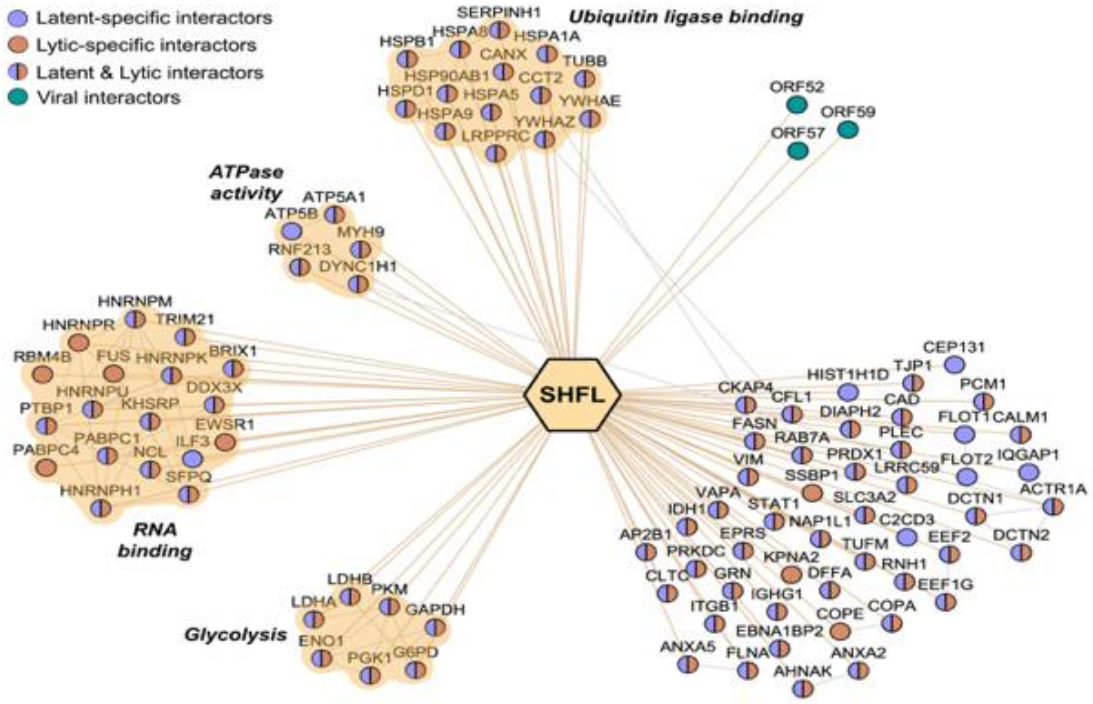

Figure 6: SHFL interactome during KSHV lytic replication. iSLK.WT cells were transfected with FLAG-SHFL and reactivated for 48 h. Through immunoprecipitation, SHFL and its interactors were pulled down and analyzed via mass spectrometry. [42]

1.6 SHFL Impact on P-body Dynamics during KSHV Infection

Our investigation began with P-bodies and stress granules, as they have emerged as prominent ribonucleoprotein (RNP) complexes. P-bodies and stress granules are involved in cytoplasmic mRNA stability and translation respectively, which are both functions that have previously associated with SHFL functionality [95-98, 90, 99-101]. To study this relationship, we applied immunofluorescence assays (IFA) to track the localization of SHFL relative to both P-body and stress granule marker proteins both inside and outside the context of KSHV infection. Strikingly, SHFL overexpression in KSHV-negative HEK293T cells revealed a significant loss in observed P-bodies as indicated by the presence/absence of canonical DDX6 foci **(Figure 7A and 7B)** [42]. This result was recapitulated within the context of KSHV

infection, using iSLK.WT cells, where we again observed a marked decline in P-body foci in response to SHFL expression **(Figure 7C and 7D)**. This observation that SHFL restricts P-body formation in the context of KSHV infection presented us with a contradictory perspective on the role of these RNA condensates during viral infection as previously reported [102]. Several groups have reported that KSHV actively restricts the formation of P-bodies during latency [103] and lytic replication [104] via the viral proteins Kaposin B (KapB) and ORF57 respectively. KSHV KapB has been linked to a specific autophagy mechanism that leads to the degradation of certain P-body components, causing what has been suggested to be active disassembly of the foci [105]. Whereas KSHV ORF57 has been linked to the blockage of *de novo* P-body formation, thus causing an apparent loss of the densities [104]. The observation that KSHV actively disassembles P-bodies, initially suggested that these cytoplasmic granules are anti-viral in function. This is further emphasized by the fact that several other DNA and RNA viruses have evolved similar strategies to also manipulate cytoplasmic RNA condensates for the promotion of viral replication [106-111, 105, 112, 104]. However, from our observations, we have identified a novel, host encoded RNA-binding protein that also stringently restricts P-bodies formation. This function of SHFL may suggest that P-body disassembly by the host may contribute to an as-yet-to-be-described cellular survival strategy in the wake of KSHV lytic infection.

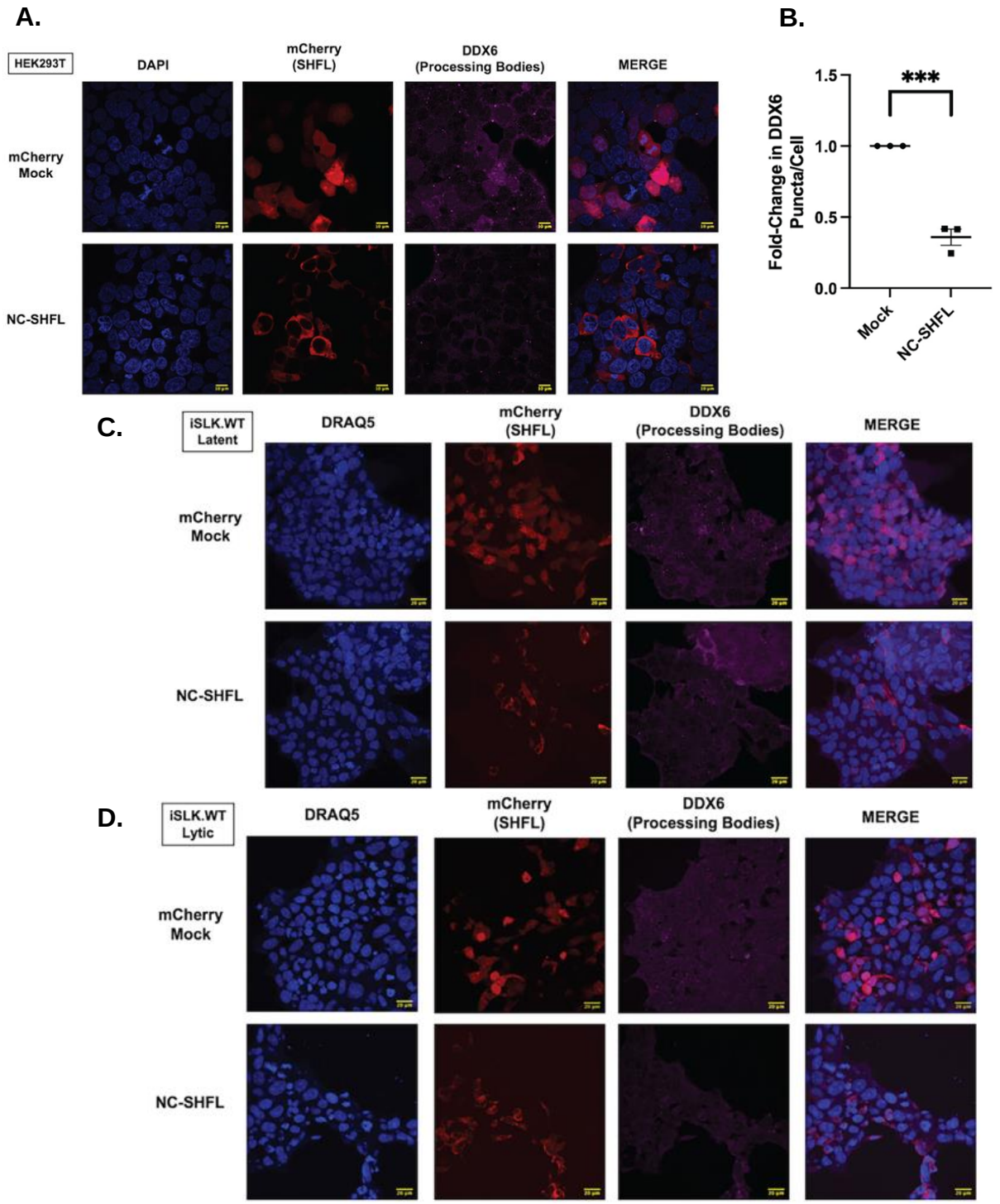

Figure 7: SHFL expression impacts RNA granule dynamics in- and outside KSHV infection. **(A).** NC-SHFL effect on P-bodies in HEK293T cells. 293T cells were transfected with either NC-EMPTY or NC-SHFL plasmids for 24 h, fixed, and stained for the P-body marker: DDX6. **(B).** P-body quantification in HEK293T cells. Microscopy images of P-bodies were quantified via imaging software, CellProfiler. **(C).** NC-SHFL effect on P-bodies in latent iSLK.WT cells. iSLK.WT cells were transfected with either NC-EMPTY or NC-SHFL plasmids for 24 h, fixed, and stained for the P-body marker: DDX6. **(D).** NC-SHFL effect on P-bodies in lytic iSLK.WT cells. iSLK.WT cells were transfected with either NC-EMPTY or NC-SHFL plasmids for 24 h, reactivated, fixed, and stained for the P-body marker: DDX6. [42]

Based upon this rationale, the overall goal of my master's thesis work is to better characterize how SHFL acts as an antiviral host factor. My central hypothesis is that SHFL regulates P-body dynamics within the cytoplasm, which directly impacts pro-inflammatory gene expression to enhance host defenses against KSHV. To address this, we first sought out to recapitulate the SHFL/P-body phenotype with FLAG-SHFL. We decided to shift SHFL models from an mCherry tag to a FLAG tag because its relative size and decreased propensity for altering structure and therefore interactions. Next, we utilized a NaAs assay to characterize whether SHFL inhibits *de novo* P-body formation or actively disassembles these granules. Following this we specifically sought to implicate the domain of SHFL that contributed to this P-body loss. We utilized a mutant library of this host factor to observe which domains failed to regulate P-bodies. After discovering two SHFL domains contributing to this granule phenotype, we posited the interaction between these regions influenced the loss through some mechanism, and that disruption of this domain interaction would inhibit SHFL effect on P-bodies. Overall, these results indicate that SHFLaa151-200 and SHFLaa251-291 form tertiary interactions that contribute to host P-body regulation through either a direct or indirect means. Ultimately, these domains of SHFL contribute to the blockage of *de novo* P-bodies, which subsequently causes an increase in select pro-inflammatory cytokine transcript levels. This impact on P-body dynamics appears to also have a significant impact on the host cell antiviral response. Deeper characterization of SHFL helps to enrich our understanding of host mechanisms for combat against KSHV infection and how cells manipulate the gene expression landscape to mitigate viral replication.

RESULTS

2.1 SHFL: Stringent Regulator of P-bodies

Though much of our group's previous SHFL/P-body findings [42] were with NC-SHFL, we decided to shift models to a FLAG-SHFL. Upon further experimentation with mCherry SHFL, we discovered that this larger tag had the potential for steric hinderance. Immunoprecipitation results suggested this, and that the bulky tag was potentially interfering with SHFL interactions. To circumvent these issues, we shifted to using a FLAG-SHFL construct and expressed it within HEK293T cells. We then sought to recapitulate the NC-SHFL P-body phenotype using this construct. FLAG-SHFL continued to significantly restrict P-bodies in both HEK293T cells and KSHV positive cells **(Figure 8A and 8B)**. After validating this SHFL phenotype to be consistent between constructs, we wanted to understand mechanistically how this ISG was influencing these RNA granules. We first sought to identify whether SHFL overexpression led to a decrease in expression of key P-body constituents. This may have been caused indirectly, such as SHFL broadly acting on transcription or translation, or through a more direct mechanism, where SHFL in some way facilitated the degradation of these protein components. Several P-body RNP components that have previously been suggested to play structural roles of the granules were analyzed: decapping mRNA 1a (DCP1A), enhancer of mRNA decapping 4 (EDC4), and dead box helicase-6 (DDX6) [82, 83, 76, 84]. These P-body constituents' expression levels were determined via immunoblot, where no noticeable differences in expression could be observed under FLAG-SHFL transfection **(Figure 8C)**. We confidently concluded that SHFL does not affect the expression of prominent P-body factors DCP1A, EDC4, or DDX6. Due to the highly dynamic nature of P-bodies and their ever-evolving characterization, we decided to not pursue P-body protein expression analysis further.

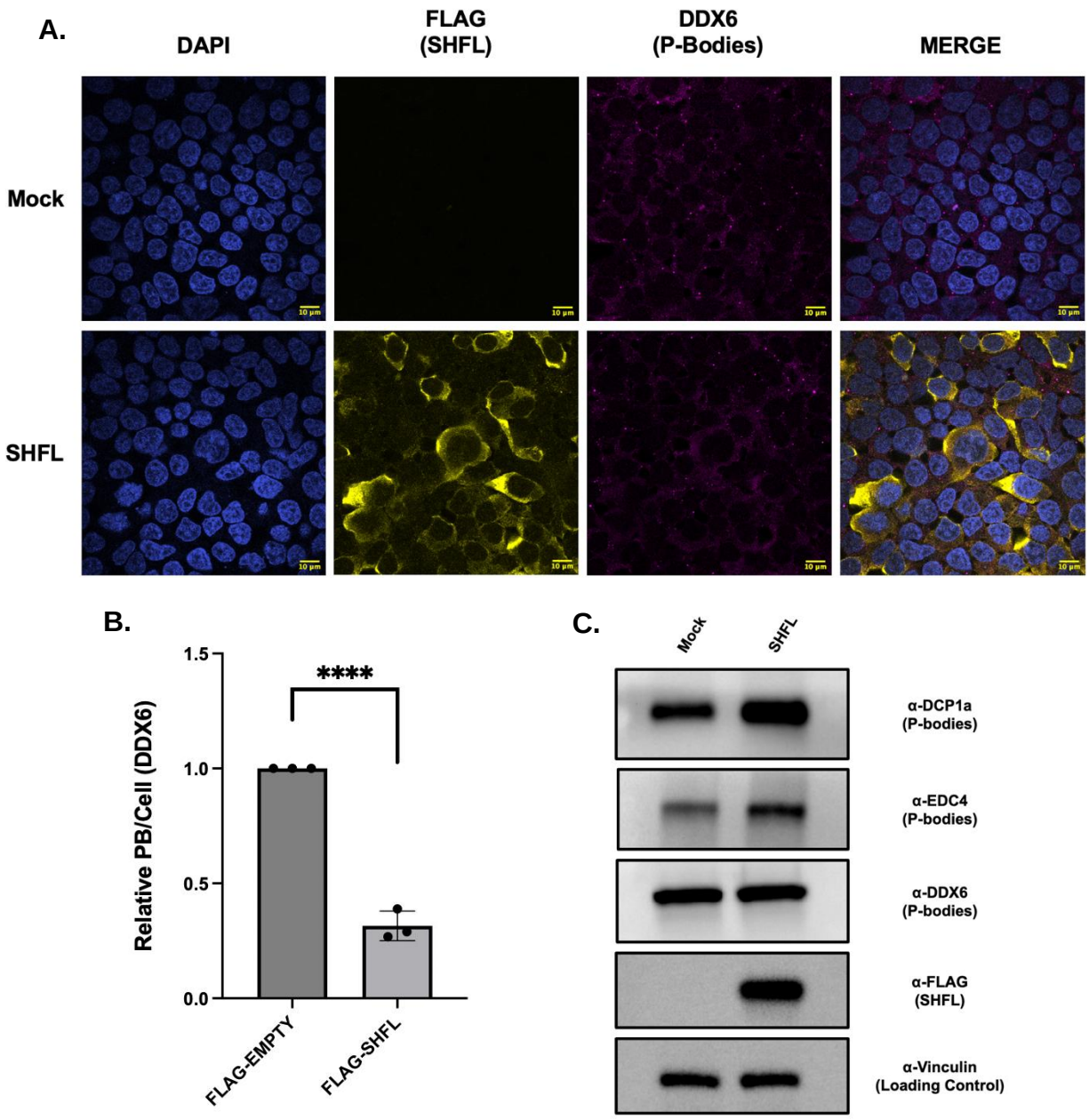

Figure 8: FLAG-SHFL expression restricts P-bodies. **(A).** FLAG-SHFL effect on P-bodies in HEK293T cells. Cells were transfected with the respective plasmids for 24 h, fixed, and then incubated with the proper antibodies for fluorescence imaging. **(B).** P-body quantification in HEK293T cells. Microscopy images of P-bodies were quantified via imaging software, CellProfiler. **(C).** Immunoblotting of HEK293T cells expressing FLAG-EMPTY or FLAG-SHFL. Cells were transfected with the indicated plasmids for 24 h, harvested, underwent SDS-PAGE and immunoblotting to determine P-body constituent expression levels.

2.2 SHFL Blocks *de novo* P-body Formation

We next sought to more broadly understand what fate these granules met resulting from SHFL expression. As previously mentioned, KSHV proteins have been observed to cause both P-body disassembly [105] and the blockage of *de novo* formation [104]. Disassembly has been characterized as the removal of specific granule constituents from existing granules. Blockage of formation has been described as a sequestration event or depletion of certain P-body factors, which prevents the forming of new foci. We set out to determine specifically how SHFL expression resulted in P-body loss. HEK293T cells were treated with sodium arsenite (NaAs), a known oxidative stressor for cells that induces a marked P-body increase, alongside SHFL transfection. A gradient of NaAs treatment was performed to best identify what working concentration could significantly increase P-body counts but minimized cytotoxicity and abnormalities in cell morphology. Based on these results, we determined that 24 h post-transfection, treatment with 0.25mM NaAs for 30 min significantly increased P-body counts and was not excessively cytotoxic. Using this NaAs assay procedure, we observed P-body numbers between mock and SHFL expressing cells. If there was no difference in P-body numbers between these conditions following NaAs treatment, this would suggest SHFL actively disassembles P-bodies. Disassembly likely takes a longer duration than 30 min, and this result could indicate that SHFL did not have enough time to cause this disassembly. If there was a difference in P-body counts between these conditions following NaAs treatment, this would suggest that SHFL blocks *de novo* P-body formation. Expression of SHFL constrains certain P-body factors that prevents the cell from utilizing them for granules even under forced P-body induction. Visually, we identified that foci were still significantly restricted by SHFL under NaAs treatment **(Figure 9A)**. P-body quantification confirmed this observation, where SHFL

expression results in P-body restriction for vehicle treated and NaAs treated cells **(Figure 9B)**. Ultimately, this result indicated to us that SHFL inhibits *de novo* P-body formation rather than actively disassembling the densities. Based upon this specific mechanism, we pursued mechanisms through which SHFL could broadly impact foci components.

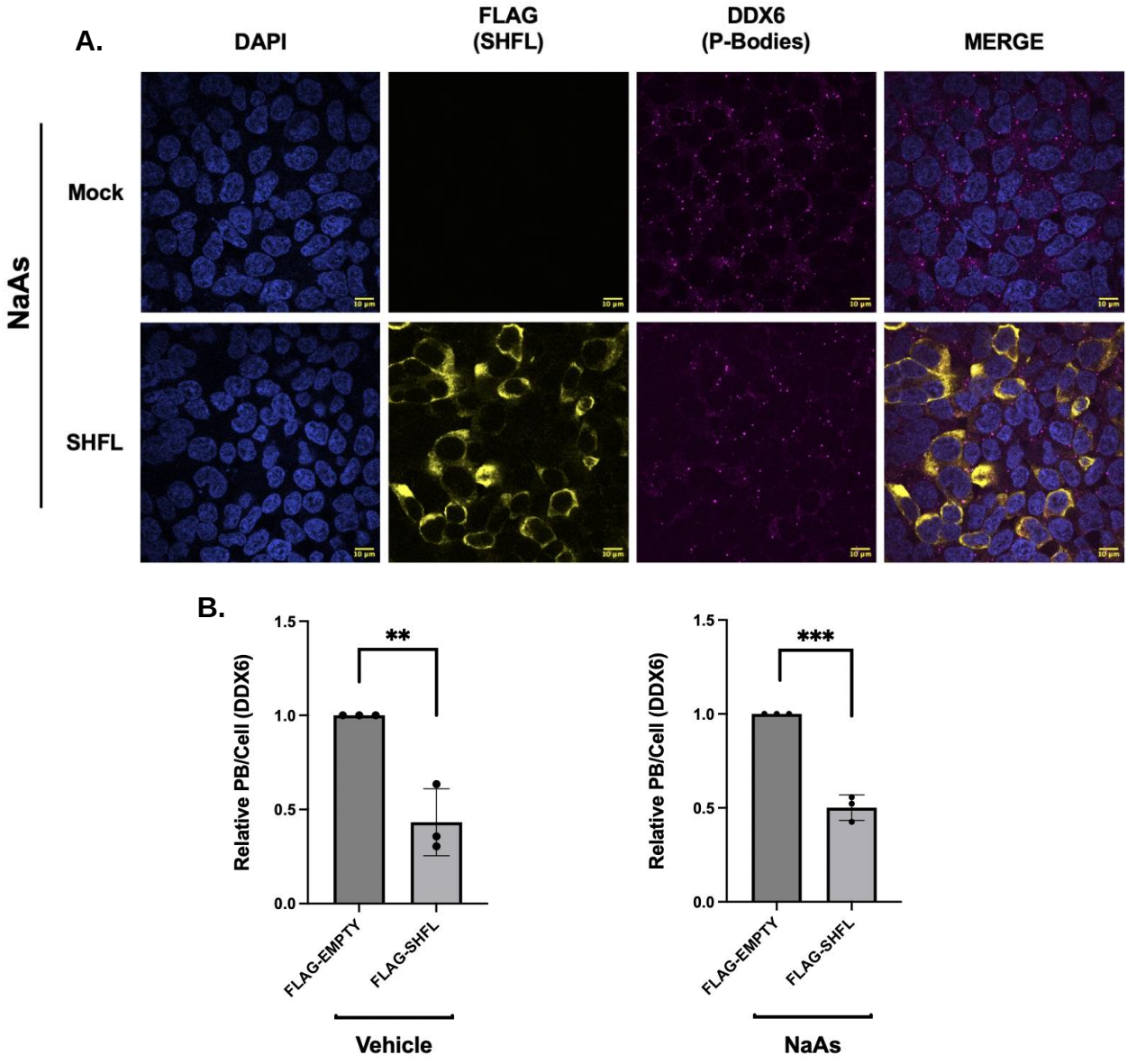

Figure 9: Shiftless restricts *de novo* P-body formation. **(A).** F-SHFL continues to restrict P-bodies in HEK293T cells during NaAs treatment. Cells were transfected with the respective plasmids for 24 h, treated with 0.25mM NaAs, fixed, and then incubated with the proper antibodies for >1 h. **(B).** Quantification of P-bodies for F-EMPTY/F-SHFL under vehicle or NaAs treatment. A CellProfiler quantification pipeline identified cytoplasmic P-body foci and counted them for analysis.

2.3 SHFL-DDX3X Interaction not critical for P-body Regulation

We next returned to the endogenous SHFL interactome **(Figure 6)** to gauge what other factors may be participating alongside Shiftless that lead to RNA granule alterations and gene manipulation. The interactor dead box helicase 3-X (DDX3X) immediately presented itself as an interesting pursuit. Though DDX3X is not often a canonical marker for P-bodies, this helicase enzyme has been implicated to be a part of these sites of translational arrest [108]. DDX3X is ubiquitous throughout eukaryotic tissues and involved in much of RNA regulation, including transcription, pre-mRNA splicing, nuclear export, and translation [113-124]. This protein can be observed to both repress global translation by preventing initiation factors from interacting [125] as well as enhance translation of certain RNAs with unique 5' UTR structures [126, 127]. Of note, several viruses, cancers, inflammatory pathways, and intellectual disabilities cause a weakened DDX3X expression, indicative of its pro-host functionality [113, 128, 129, 121, 130]. Before investigating the potential effects SHFL had on DDX3X, we first needed to confirm this interaction via co-immunoprecipitation **(Figure 10A)**. Following this confirmation of a SHFL-DDX3X interaction, we wanted to identify if expression levels were altered. As seen in **Figure 10B**, SHFL over-expression did not lead to a decrease in DDX3X protein levels. Next, we observed DDX3X localization and expression through fluorescence microscopy. As expected, the protein was diffusely cytoplasmic; there were no noticeable differences in localization, densities, or puncta **(Figure 10C)**. Based on the immunoblotting and immunofluorescence results, this interaction did not appear to have direct contributions to the SHFL/P-body phenotype. Thus, we deiced to pursue alternative phenotypes and mechanisms that SHFL induces.

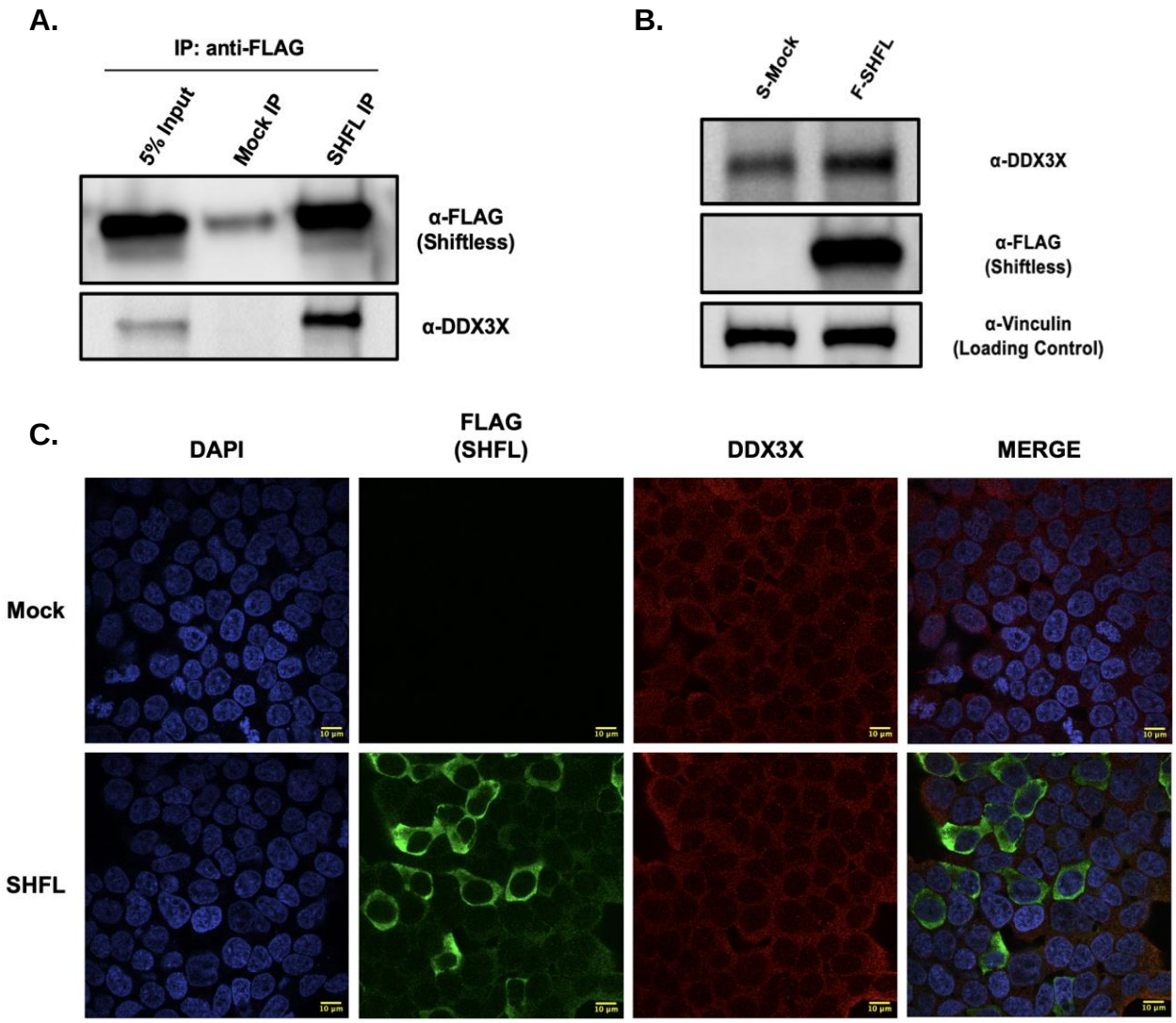

Figure 10: SHFL expression does not significantly alter interactor, DDX3X. **(A).** Immunoprecipitation confirms SHFL-DDX3X interaction. Pull down of F-SHFL and subsequent immunoblotting reveals DDX3X as a SHFL interactor. **(B).** Immunoblotting reveals DDX3X expression levels during SHFL expression. Cells were transfected with F-EMPTY or F-SHFL for 24 h, harvested, subject to SDS-PAGE and immunoblotting to determine DDX3X expression levels. **(C).** Confocal microscopy of DDX3X expression and localization. Cells were transfected with the respective plasmids for 24 h, fixed, and then incubated with the proper antibodies for >1 h.

2.4 SHFL RNA Binding Domain not Responsible for P-body Loss

Based on the previous result that SHFL blocks *de novo* P-body formation, we desired to identify how this occurs mechanistically. While our previous efforts focused on candidates that could be affected, we shifted our observation to SHFL itself instead of these potential protein

interactors. Since SHFL has been previously classified and studied as an RNA binding protein [41], we desired to analyze if this function either directly or indirectly related to the P-body phenotype. After observing no impact on certain P-body protein constituents, we posited that SHFL impacted the other biomolecule comprising these granules: RNA. Practically, this could involve SHFL sequestering certain mRNAs away from translation complexes. Or, SHFL could increase rates of degradation or decrease transcription levels, which could reduce the availability of RNAs and thus prevent *de novo* formation of P-bodies. As previously mentioned, the domain 102-150aa, termed the 'PABPC binding domain', is responsible for SHFL- Poly-A Binding Protein Cytoplasmic 1 (PABPC1) interaction, as well as housing the predicted region for its RNA binding ability. The arginine residues R131, R133, and R136 have been implicated as the critical amino acids for RNA binding [41]. Two mutants were constructed via infusion cloning: FLAG-SHFLΔ102-150 (termed 'FLAG-SHFLΔRBD') and FLAG-SHFLΔR131A, R133A, R136A (termed 'FLAG-SHFLΔ3R'). The second mutant, FLAG-SHFLΔ3R, ought to serve as a highly specific mutant that lacked the ability to bind to RNA with minimal structural and interactive difference. Whereas, the first mutant, FLAG-SHFLΔRBD, serves as a redundancy to eliminate RNA binding ability but in a less specific manner. Confirmational analysis via RNA immunoprecipitation verified that FLAG-SHFLΔRBD and FLAG-SHFLΔ3R were indeed deficient in RNA binding. Using fluorescence microscopy, both mutants were expressed alongside SHFL and Mock transfected cells **(Figure 11C)**. P-body quantification revealed that not only did full length SHFL significantly reduced P-bodies, but FLAG-SHFLΔRBD and FLAG-SHFLΔ3R did as well **(Figure 11A & 11B)**. These results indicated that SHFL RNA binding ability was not the immediate cause of P-body loss. Of note, this did not definitively eliminate a SHFL impact on RNA as a cause for P-body loss; it simply shows that SHFL ability

to bind to RNA is not what is responsible for P-body loss. This distinction is important because it preserves the possibility of SHFL impacting RNA in other facets, which remain to be explored.

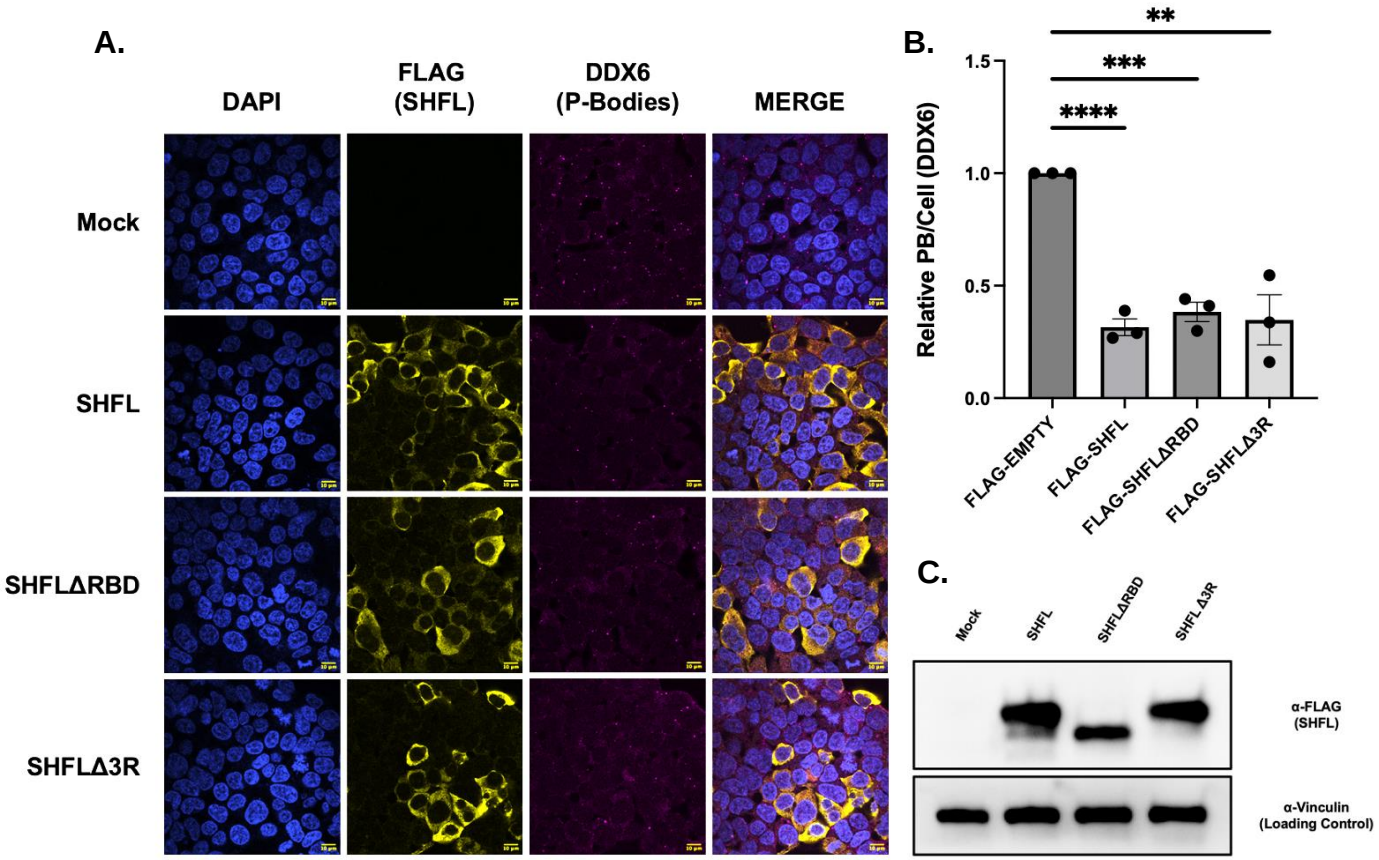

Figure 11: SHFL RNA Binding Domain not responsible for P-body disruption. (**A).** F-SHFLΔRBD and F-SHFLΔ3R also restrict P-bodies in HEK293T cells. Cells were transfected with the respective plasmids for 24 h, fixed, and then incubated with the proper antibodies for >1 h. **(B).** Quantification of P-bodies between F-EMPTY, F-SHFL, F-SHFLΔRBD and F-SHFLΔ3R expression with and without NaAs treatment. A CellProfiler quantification pipeline identified cytoplasmic P-body foci and counted them for analysis. **(C).** Immunoblotting of SHFL and its RNA binding mutants. HEK293T cells were transfected with F-EMPTY, F-SHFL, F-SHFLΔRBD and F-SHFLΔ3R for 24 h, harvested, and subject to SDS-PAGE/immunoblotting to confirm expression.

2.5 SHFL Mutant Library Reveals Culpable P-body Domains

After identifying that SHFL ability to bind to RNA did not directly contribute to the loss of P-bodies, we next decided to uncover which domain(s) of this protein were responsible for this phenotype. An alternative aim of this pursuit was to also find a null mutant of SHFL that

could not restrict P-body formation. To help achieve this, we used six mutants of SHFL, where 50aa truncations were made systematically. A previous graduate student in the lab had cloned both an N-terminus SHFL mutant library and a C-terminus mutant library, where 50aa deletions were made starting at each respective end. The final six mutants chosen for study were: FLAG-SHFLΔ1-50, FLAG-SHFLΔ1-100, FLAG-SHFLΔ1-150, FLAG-SHFLΔ1-200, FLAG-SHFLΔ1-250, and FLAG-SHFLΔ241-291 **(Figure 12A)**. Using these constructs, we hypothesized that once the SHFL domain responsible for the P-body phenotype was lost, there would be no significant loss of P-bodies for that mutant or subsequent ones. It was observed that significant loss of P-bodies can be seen until amino acids 151-200 are truncated **(Figure 12B & 12C)**. Interestingly when the next mutant (FLAG-SHFLΔ1-250) was expressed, a significant loss in P-bodies can be seen once again **(Figure 12B & 12C)**. But, when the C-terminal 50aa of SHFL was truncated solely, no loss in P-bodies can be observed **(Figure 12B & 12C)**. This result suggests that domains 151-200 and 251-291 both affect P-bodies. When 151-200aa were absent, there was no P-body loss. When 201-250aa was deleted, but 151-200aa continue to be absent, there was once again a significant P-body loss. When only 241-291aa were truncated, but 151-200aa still remain within SHFL, there was no significant P-body loss. Of note, the C-terminal domain also contains the nuclear export signal (NES), meaning that SHFL could simply be trapped in the nucleus, unable to function due to altered localization. Based on these results, we hypothesized that either 1. SHFL has dual functioning domains, where 151-200aa and 241-291aa potentially interact with one another, or act as a redundancy system. Or, 2. SHFL functional domain is 151-200aa, but SHFL localization is critical for functionality as well.

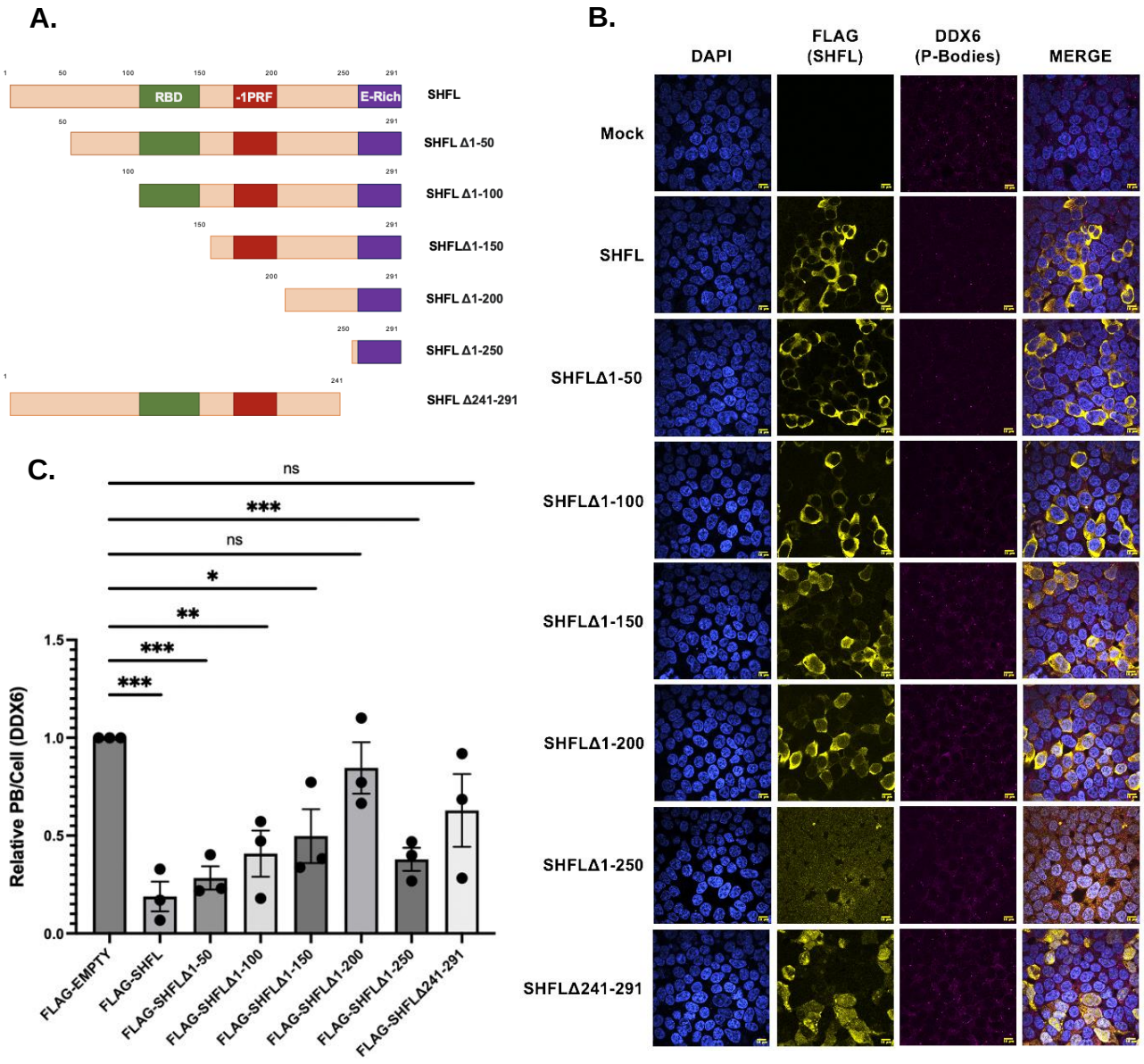

Figure 12: SHFL Library reveals two contributary domains linked to P-body phenotype. **(A).** Schematic of the SHFL mutant library. SHFL mutants were cloned via deletion mutagenesis, where 50 aa truncations were made systematically. **(B).** F-SHFL mutant library impact on P-bodies. Cells were transfected with the respective plasmids for 24 h, fixed, and then incubated with the proper antibodies for >1 h. **(C).** Quantification of P-bodies for the each SHFL mutant. CellProfiler quantification provided an unbiased identification of cytoplasmic P-body foci to help determine which SHFL domain impact this phenotype.

2.6 SHFL P-body Mutants Confirm Multi-Domain Functionality

Based on the results in **Figure 12**, we created more specific SHFL mutants via infusion cloning to better understand which specific domain(s) of SHFL were causing this P-body phenotype. Another aim of this study was to identify one, highly specific SHFL null mutant that could be used in comparison to full length FLAG-SHFL. This null mutant could provide the necessary contrast to identify and/or confirm SHFL interactors that may be contributing this P-body phenotype and broader SHFL functionality. Five mutants were then constructed: FLAG-SHFLΔNES (L261A, L264A, L267A, L269A), FLAG-SHFLΔ151-200, FLAG-SHFLΔ151-200 + NES, FLAG-SHFLΔ151-200, 251-291, and FLAG-SHFLΔ251-291 and expressed in HEK293T cells **(Figure 13A)**. The mutant with the non-functional NES ought to limit SHFL to the nucleus, which could help to identify if localization impacts functionality. If nuclear export is necessary for P-body restriction, we would anticipate this mutant to have no significant loss in P-bodies. We anticipated that the single domain deletions (i.e. FLAG-SHFLΔ151-200 and FLAG-SHFLΔ251-291) and double domain deletion (FLAG-SHFLΔ151-200, 251-291) would result in no significant loss in P-bodies, since we observed as much with the SHFL mutant library. Finally, to note, the C-terminal deletion was shortened by 10aa in both the single and double domain truncations. With the SHFL mutant library immunofluorescence results, we observed that FLAG-SHFLΔ1-250 led to significant loss in P-bodies and FLAG-SHFLΔ241-291 led to no significant loss in P-bodies. The 10aa overlap between the two mutants did not significantly impact the phenotype to result in restriction or a lack thereof. We concluded that we could safely neglect these residues in our new mutants. Once again, cells were transfected, fixed, stained with immunofluorescent probes, and imaged via confocal microscopy. First, image analysis revealed rather interesting results about SHFL localization. FLAG-SHFLΔNES remained cytoplasmic

despite its mutated lysine residues **(Figure 13B)**. FLAG-SHFLΔ151-200, and FLAG-SHFLΔ251-291 also remained cytoplasmic **(Figure 13B)**. Strikingly, FLAG-SHFLΔ151-200 + NES and FLAG-SHFLΔ151-200, 251-291 were both nuclear **(Figure 13B)**. These localization observations alone suggest that SHFL likely interacts with other proteins that allow for nuclear export through an uncharacterized mechanism, where the NES and 151-200aa domain must be non-functional for cytoplasmic presence to be reduced.

Second, P-bodies were quantified for each potential SHFL null-mutant. FLAG-SHFLΔNES significantly restricted P-body foci post 24 h **(Figure 13B & 13C)**. FLAG-SHFLΔ151-200, FLAG-SHFLΔ251-291, and FLAG-SHFLΔ151-200, 251-291 did not result in any significant P-body loss **(Figure 13B & 13C)**. Strangely, FLAG-SHFLΔ151-200 + NES led to a significant loss of P-body foci **(Figure 13B & 13C)**. Although this restriction was not as drastic as we normally observe for FLAG-SHFL, it is significant, which presents quite an interesting case among these mutants: nuclear SHFL with some ability to continue to restrict P-bodies. Wholistically, this quantification helped identify that SHFL localization alone is not enough to lead to the P-body phenotype. This resulted in our group pursuing the alternative hypothesis: SHFL domains 151-200aa and 251-291aa both have functional capacity. Both domains clearly impact the loss of P-bodies through some mechanism, as their loss results in no restriction of foci **(Figure 13B & 13C)**. Also of note, this is not a functionally redundant system as previously hypothesized. If both domains functioned independently of one another, we would anticipate a significant loss of P-bodies for the single domain mutants and only no P-body loss for the double domain mutant. However, that was not what we observed. When we deleted either

domain, we saw that SHFL lost the ability to restrict P-bodies. This led us to conclude that these two domains act dependently upon one another.

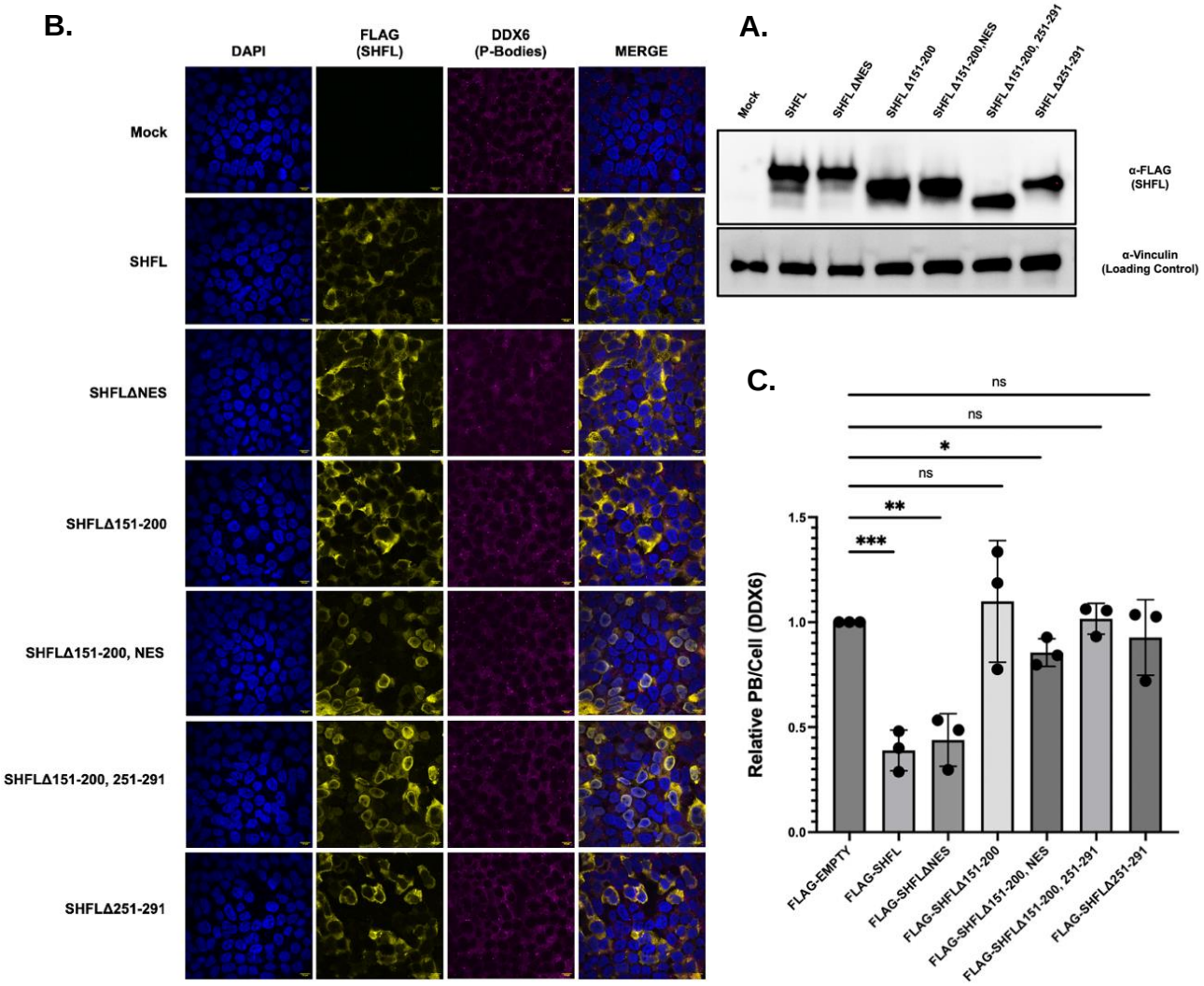

Figure 13: SHFL/P-body mutants confirm dual domain co-functionality. **(A).** Immunoblotting of HEK293T cells expressing SHFL/P-body mutant vectors. Cells were transfected with the indicated plasmids for 24 h, harvested, and subject to SDS-PAGE/immunoblotting to confirm expression. **(B).** Fluorescence microscopy images of SHFL/P-body mutants. Cells were transfected with FLAG-EMPTY, FLAG-SHFL, FLAG-SHFLΔNES (L261A, L264A, L267A, L269A), FLAG-SHFLΔ151-200, FLAG-SHFLΔ151-200 + NES, FLAG-SHFLΔ151-200, 251-291, or FLAG-SHFLΔ251-29. for 24 h, fixed, and then incubated with the proper antibodies for >1 h. **(C).** Quantification of P-bodies for SHFL/P-body mutants. CellProfiler quantification provided an unbiased identification of cytoplasmic P-body foci and counted them for analysis.

DISCUSSION

3.1 SHFL Domain Interaction Critical for Functionality

During KSHV lytic replication, certain transcripts possess the necessary RNA structural elements to evade viral endonuclease cleavage and host exonuclease decay. SHFL is one of these escapees and has been shown to serve an antagonistic role during KSHV infection. In the characterization of this host factor, SHFL has been observed to not only restrict KSHV, but also restrict cytoplasmic P-body levels. We postulated that this RNA granule loss may contribute to its anti-viral functionality. To probe this, we needed to better understand how SHFL regulated P-bodies. Thus, we utilized a NaAs assay to observed that SHFL inhibits *de novo* P-body formation. To determine which domain of SHFL were critical to this phenotype, we expressed a mutant library of this host factor to observe which 50aa domains could not block P-body formation. We identified that two different domains of SHFL had the ability to affect this phenotype and aim to better understand how this restriction mechanism occurs. Ultimately, SHFL/P-body regulation and the broader impact on viral replication remains to be fully understood. However, several recent observations have illuminated different avenues that may be fascinating for future study. Through continued characterization of this anti-viral protein, hopefully we will (1.) identify a novel mechanism for P-body regulation, (2.) determine the extent of this impact on P-bodies during KSHV infection, and (3.) understand in its totality how SHFL opposes viral parasites.

3.1.1 SHFLΔGW cannot significantly Restrict P-body Formation

To better understand the interplay between the two domains of SHFL implicated in the P-body phenotype, we used DeepMind's protein structure prediction software AlphaFold (https://alphafold.ebi.ac.uk/). Though these domains are not sequentially neighboring; they are

predicted to be very close to one another spatially. SHFL 151-200aa and 251-291aa even potentially share a pocket on the periphery of the structure that could potentially serve as a platform to facilitate interactions. This site of merging domains could very well be the region of SHFL that allows for an alternative nuclear export mechanism as well as for the restriction of P-bodies. The arrow in **Figure 14** denotes the potential site for where the two domains interact with one another and form a scaffold for other proteins. Interestingly, the protein prediction software pinpoints these two domains to interact through one hydrogen bond only directly between residues W191 and G259 **(Figure 14A)**. We posited that if the interaction between these two residues is broken, SHFL may lose degrees of functionality. Though SHFL has not been characterized to have any enzymatic activities, these domains may serve as a scaffold for interactors. If this hypothesis of interdependent domain functionality can be validated via *in vitro* assays, it would represent a structural and functional novelty for Shiftless. To address these hypotheses, we first created FLAG-SHFLΔW191A, G259A (termed FLAG-SHFLΔGW) to disrupt the interactions between these domains **(Figure 14B)**. Interestingly, we observed that this mutant does not result in a significant reduction of P-bodies **(Figure 14C and 14D)**. P-bodies present during FLAG-SHFLΔGW expression typically appeared smaller in size than normal P-body foci. Ultimately, these findings support the hypothesis that these two domains interact at this juncture, and it contributes, at least partially, to SHFL functionality. The specific mechanisms in which this two-residue mutant disrupts SHFL interactions remain to be further characterized.

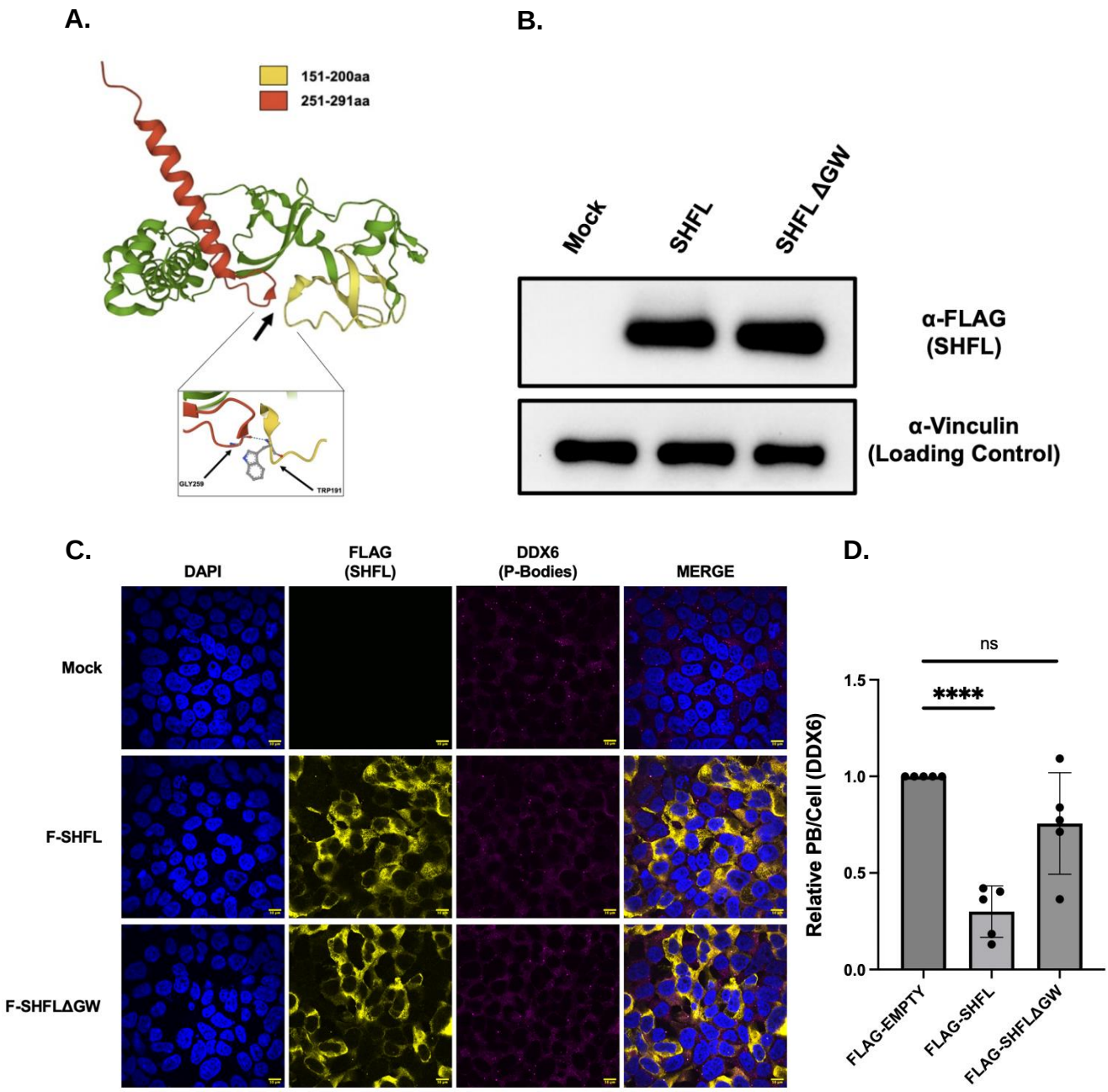

Figure 14: SHFLΔGW sufficient to inhibit P-body blockage. **(A).** SHFL predicted Alphafold structure with P-body domains. Highlighted in red (151-200 aa) and yellow (251-291 aa) are the two domains to show an impact on P-body dynamics. The two domains are shown to only, directly interact with one another via residue W191 and G259. **(B).** SHFLΔGW expression via immunoblot. HEK293T cells were transfected with the indicated plasmids, harvested and subject to SDS-PAGE/immunoblotting. **(C).** SHFLΔGW expression via immunofluorescence and its effect on P-bodies. Following 24 h expression of the plasmids, P-bodies were observed via immunofluorescence. **(D).** SHFLΔGW P-body quantification. CellProfiler quantification provided an unbiased identification of cytoplasmic P-body foci and counted them for analysis.

3.1.2 SHFL Domain Interaction Impacts KSHV Lytic Replication

Interestingly, regarding KSHV infection, the deletion of these two domains appears to significantly impact viral replication. To determine the impact of these domains on the antiviral capacity of SHFL, we next knocked down endogenous SHFL in KSHV infected iSLK.219 cells, complimented with the expression of several SHFL mutants including F-SHFLΔ151-200, F-SHFLΔ151-200, 251-291, and F-SHFLΔ251-291 and monitored the efficiency of lytic reactivation for 72 hours **(Figure 15A)**. RFP (KSHV positive) cells were quantified to capture the efficiency of viral reactivation and replication **(Figure 15B)**. When either both domains were deleted or the C-terminal domain was removed, KSHV reactivation was significantly heightened. From this experiment, we found that loss of both the 151-200 and the C-terminal domains of SHFL or the C-terminal domain alone resulted in loss of SHFL functionality. These results suggest that the ability of SHFL to restrict P-body formation is tied to its anti-KSHV capacity. Further characterization of SHFL anti-viral mechanisms remain to be explored.

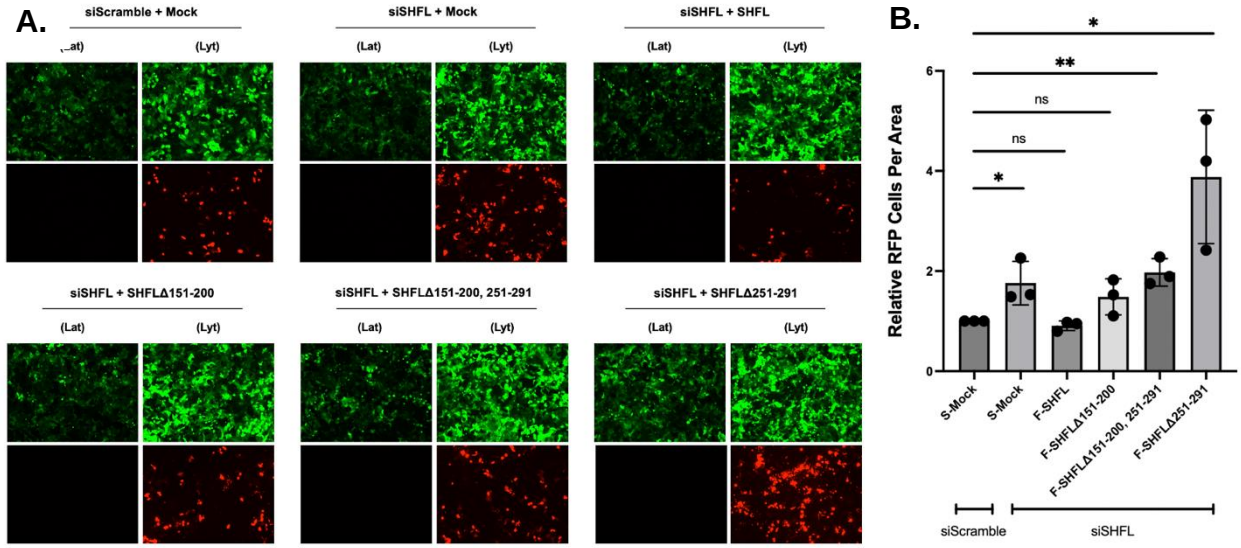

Figure 15: SHFL/P-body mutants enhance KSHV lytic reactivation. **(A).** siSHFL + SHFL/P-body mutants enhance KSHV reactivation. iSLK.219 cells were either treated with siSCRMABLE or siSHFL then transfected with F-EMPTY, F-SHFL, or one of the F-SHFL P-body mutants. Following 72 h of reactivation, fluorescence was captured via confocal microscopy. **(B).** Quantification of RFP cells for F-SHFL P-body mutants. 5 independent and randomized views were captured for the above conditions. RFP expression (reactivated cells) was quantified.

3.2 SHFL P-body Restriction Mechanism

Regarding the specific mechanism through which SHFL blocks *de novo* P-body formation, SHFL either directly interacts with P-body constituents and disrupts their scaffolding or otherwise impedes their expression likely at the translation level. Interestingly, from the P-body dynamics of the SHFL RNA binding mutants **(Figure 11)**, we are confident that this functionality is not culpable for P-body loss. Several groups have observed SHFL localizes to P-bodies and Stress Granules, suggesting that a direct interaction with these RNA granule types exist [38, 40]. Previous work has shown that P-body disassembly can be triggered by loss of critical scaffolding components such as LSm14a [136, 137], DDX6 [137, 138], or EDC4, which have all been shown to lead to losses in these foci [139]. The loss of these factors suggest that P-body regulation can occur by critically altering protein expression, which affects the scaffolding of these densities. Alternatively, the expression and phosphorylation of the polypeptide NBDY has been shown to cause the loss of P-bodies, by potentially disrupting the electrostatic networks of these granules [140, 141]. This polypeptide has been linked to an interaction with P-body factor, DCP2, providing insight into this mechanism of regulation [141]. From our previous IP-MS of SHFL, there are several interactors that remain to be explored that could inform any one of these mechanisms. Especially as many SHFL interactors are known P-body constituents [42]. SHFL also interacts with several Ubiquitin-ligase binding proteins, suggesting it may also be a factor that recruits E3 ligases to ubiquitinate target RBPs and therein indirectly influences their regulation. Alternatively, SHFL may act more broadly to cause P-body loss. We observed that SHFL expression results in a global translation increase **(Figure 16A)**. This translational cascade may alter RNA stability within the cytoplasm, which ultimately leads to less nucleation of *de novo* P-bodies.

Ultimately, using either a highly specific SHFL mutant (i.e. FLAG-SHFLΔGW) or one of the null mutants validated above, we will begin to identify the key interactors of SHFL that lead to its influence over P-body formation via further application of immunoprecipitation based mass spectrometry (IP-MS). This comparison would potentially reveal missing interactors or groups of interactors between FLAG-SHFL (that can cause P-body loss) and the non-functional SHFL mutant (that cannot lead to P-body loss). As observed in **Figure 8**, three P-body components were checked for decreased expression during SHFL overexpression. However, P-bodies are dynamic entities that are continuously being further characterized and the composition of P-bodies can vary between cell types. Thus, there remains many other known P-body constituents whose expression could be impacted by SHFL that are yet to be identified.

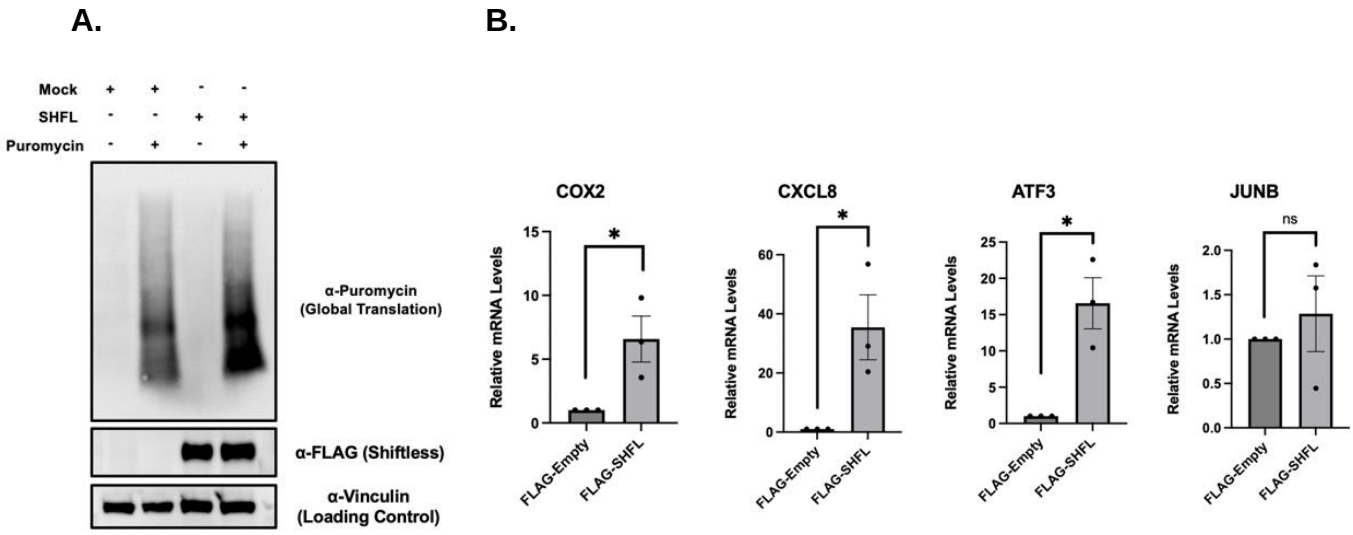

Figure 16: SHFL enhances global translation and ARE-mRNA levels. **(A).** Surface Sensing of Translation (SUnSET) Assay during SHFL expression. HEK293T cells were then transfected with either a mock or FLAG-tagged SHFL vector. 24h later, total protein extracts were harvested, and viral protein expression analyzed via Immunoblot. **(B).** Relative transcript levels of ARE-mRNAs during SHFL expression. HEK293T cells were transfected with the indicated plasmids, treated with 10ng/mL TNFα for 24 h, harvested and subject to RT-qPCR.

3.3 Uncovering SHFL Anti-viral Nature

SHFL and other ISGs, are critical pieces of the grand evolutionary war that wages between human hosts and viral pathogens. As we and other have observed, SHFL serves an anti-viral role during KSHV infection as well as several other viruses [38-42, 21, 43, 44, 29, 45, 36, 46]. Among the many mechanisms that SHFL restricts viral replication, SHFL has been shown to restrict the translation of several flaviviruses [39, 43]. To better understand how this could be related to its influence over KSHV replication and P-body formation, we also investigated SHFLs impact on global translation. Using a surface sensing of translation (SUnSET) assay, we were able to observe a marked increase in global translation for HEK293T cells expressing SHFL **(Figure 16A)**. The SUnSET assay involves treating cells with puromycin, a tRNA mimic, that labels actively translating peptide chains and terminates their translation. During the 20 min of treatment with either vehicle control (dH2O) or Puromycin (10 ug/ml), peptide conjugates of various sizes form within the cytoplasm of cells and can be measured for an understanding of broad-scale translation rates. This observation is in-fact contrary to that found in the first SHFL report by Suzuki et al, where they found no impact of SHFL expression on global gene expression using the same assay in HepG2 cells [43]. This suggests that there may be cell type specificity involved in the capacity of SHFL to influence global translation and perhaps global RNA dynamics therein. Since P-bodies are often implicated as sites of translational arrest and RNA storage, their loss under SHFL expression ought to alter the availability of certain transcripts. Transcripts with AU-rich elements (ARE) often encode for pro-inflammatory cytokines and can thus be tied to the inflammatory response. It has been widely observed that P-body presence correlates to a decrease in ARE-mRNA abundance, and a loss in P-bodies associates with an increase in this class of transcript's levels [131, 103, 132-135]. We wanted to

identify if this observation was conserved in the context of SHFL expression. We transfected cells with SHFL, treated them with purified TNF-a (to induce ARE-mRNA expression), and analyzed the abundance of select ARE-mRNAs. Interestingly, we found that several of these genes had increased transcript levels **(Figure 16B)**. Therefore, we postulate that as SHFL induces a loss in P-body foci within the cytoplasm, this decreases the amount of turnover or at the very least ends stasis of certain transcripts, some of which are directly related to the immune response. Collectively, these results call for further investigation into novel facet of SHFL function and how it links to previously reported SHFL phenotypes.

SHFL is a fascinating candidate for understanding this novel tripartite interface between RNA fate, the innate immune response and viral infection. The ability for a protein to regulate RNA granules is quite rare within the human proteome and suggest there are likely many others that allow the cell to modulate these dynamic RBP condensates. Our continued characterization of SHFL will undoubtedly expand our understanding of how human cells have evolved such multifaceted tools for combating viral agents.

MATERIALS AND METHODS

4.1 *Cell Culturing and Transfection*

HEK293T cells (ATCC) alongside our KSHV-infected renal carcinoma human cell lines iSLK.BAC16 (iSLK.WT) and iSLK.219 were grown in Dulbecco's modified Eagle's medium (DMEM; Invitrogen) supplemented with 10% fetal bovine serum (FBS) and 1% Penicillin/Streptomycin (PenStrep). Both KSHV positive cell lines contain a doxycycline-inducible RTA promoter that lead to lytic reactivation upon treatment with 1μg/mL doxycycline (BD Biosciences) and 1mM sodium butyrate for 48-72 hrs.

DNA transfections were conducted with the transfection reagent PolyJet (SignaGen) upon cells that were >70% confluent for 24 hrs. Reverse transfections with small interfering RNA (siRNA) were performed using INTERFERin (Polyplus Transfection) and 10μm siRNAs. siRNAs were ordered via IDT as Dicer-substrate siRNA (DsiRNA; siRNA C19ORF66, hs.Ri.C19orf66.13.1).

4.2 *Cloning*

The FLAG-C19ORF66/FLAG- SHFL vector was obtained by a former graduate student within the lab, who ordered the C19ORF66 coding region as a G-block from IDT and cloned it in a pcDNA4 Nter-3xFlag vector. Using deletion mutagenesis, the aforementioned graduate student cloned the SHFL mutant library of 50aa truncations starting from the N-terminus as well as the converse mutant library where the systematic deletions were made starting from the C-terminus. From the full-length SHFL, the same graduate student also generated a SHFL deletion mutant lacking amino acids 102-150 (FLAG-SHFLΔ102-150). The FLAG-SHFLΔRB was ordered as a G-Block from IDT with the 3 point mutations R131A, R133A, and R136A and cloned into a pcDNA4 Nter-3xFlag vector. The mutants FLAG-SHFLΔNES and FLAG-SHFLΔ151-200 +

NES were also ordered from IDT as G-Blocks with the point mutations L261A, L264A, L267A, and L269A and cloned into pcDNA4 Nter-3xFlag vectors. Alongside these, FLAG-SHFLΔ151-200, FLAG-SHFLΔ151-200, 251-291, FLAG-SHFLΔ251-291, and FLAG-SHFLΔT191A, G259A were ordered as G-Blocks from IDT and cloned into a pcDNA4 Nter-3xFlag vector. G-Blocks were cloned into the vector backbones via in-fusion cloning (Clonetech-takara); all final constructs were verified via Sanger Sequencing.

4.3 *Immunofluorescence*

HEK293T or iSLK.WT cells were grown on 10mm, circular coverslips with transfections and reactivation to follow (dependent upon the experiment). Cells were then fixed with 4% formaldehyde for 30min at room temperature. Subsequently, they were permeabilized in 1% Triton X-100 and 0.1% sodium citrate in phosphate-buffered saline (PBS) for 10 min, blocked in bovine serum albumin (BSA) for 30 min, and incubated with the proper antibodies at the recommended dilutions for 1 h. Following this, cells were washed in phosphate buffer saline (PBS) and incubated with Alexa Fluor secondary antibodies 488, 594, 680 (Invitrogen) at a 1:1500 dilution for 1 h. After another wash with PBS, coverslips were mounted using DAPI Vectashield mounting medium (Vector Labs), which stained nuclei for visualization in the 350nm wavelength. All coverslips were visualized via confocal microscopy with a Nikon A1 resonant scanning confocal microscope (A1R-SIMe).

4.4 *RNA Granule Quantification*

Processing bodies were quantified using an unbiased image analysis pipeline generated in the freeware CellProfiler (cellprofiler.org); the template for this specific pipeline was shared with us by collaborators at the University of Toronto. The analysis begins with detection and defining of the cells nuclei via the DAPI (350nm) channel, which occurs by applying a binary threshold to

the image and requesting detection of objects between 40 and 200 pixels. Based on each defined nuclear object, the “Propagation” function analyzes the 488nm channel image (identifying FLAG-SHFL) to identify transfected cell borders. The pipeline would then subtract out the nuclei from the total area defined for cells to define the cytoplasmic spaces. Using this cytoplasmic mask, the 594nm channel image, with the fluorescing P-body puncta (stained with DDX6, EDC4, or DCP1a), could be overlayed to only identify cytoplasmic foci (i.e. excluding any nuclear signals). The “Enhance Speckles” function reduced background staining in the cytoplasmic channel. The “global thresholding with robust background adjustments” function would specifically define and denote certain puncta based upon strict size and intensity ranges, so as to reduce the amount of background artifacts quantified. All size and intensity ranges and thresholds throughout the pipeline remained unchanged between experiments. Those puncta of specific size and intensity were quantified and used for data analysis.

4.5 *Immunoblotting*

After cells were harvested, the samples were subjected to centrifugation at 3000rpm for 3-5 min at 4°C. The pellets were washed with PBS and prepared in lysis buffer (NaCl, 150 mM; Tris, 50 mM; NP-40, 0.5%; dithiothreitol [DTT], 1 mM; and protease inhibitor tablets). After 20 min, lysates were spun down at 10,000rpm for 10 min at 4°C. A Bradford assay then helped determine the biomolecular density of each supernatant. Equal amounts of sample were then resolved via SDS-PAGE and immunoblotted with the respective antibody at the recommended dilution, typically 1:1000, in TBST (Tris-buffered saline, 0.1% Tween 20). Membranes were subjected to a primary antibody incubation for >16 h, followed by a >1 h secondary antibody incubation with horseradish peroxidase (HRP)-conjugated goat anti-mouse or goat anti-rabbit at a 1:5000 dilution (Southern Biotechnology).

4.6 *RT-qPCR*

Cells were harvested and were subjected to centrifugation at 3000rpm for 3-5 min at 4°C. Pellets were treated with TRIzol based on the manufacturer's recommended protocol to extract total RNA for each sample. Using 1µg of total RNA, cDNAs were synthesized via the AMV reverse transcriptase (Promega) and directly subject to quantitative PCR (qPCR). The SYBR green qPCR kit (Bio-Rad) was used for cDNA analysis, where signals were normalized to 18S unless otherwise specified.

4.7 *RNA Immunoprecipitation (RIP)*

After the respective, experimental transfections, cells were crosslinked in 1% formaldehyde for 10 mins, quenched in 125mM glycine, and washed in PBS. Samples were then thoroughly lysed via treatment with a low-salt lysis buffer [NaCl 150mM, NP-40 0.5%, Tris pH8 50mM, DTT 1mM, MgCl2 3mM containing protease inhibitor and RNase inhibitor] followed by sonication. Following centrifugation and removal of cell debris, Magnetic G-coupled beads or anti-FLAG M2 Magnetic Beads were added to the samples and incubated overnight at 4°C. The next day, the beads were washed three times with lysis buffer and twice with high salt-lysis buffer, which was the low-salt lysis buffer with the exception of 400mM NaCl. Samples were separated into two fractions: 1. A sample of beads resuspended in 30µL lysis buffer used for immunoblotting 2. A sample of beads resuspended in Proteinase K buffer (NaCl 100mM, Tris pH 7.4 10mM, EDTA 1mM, SDS 0.5%) containing 1µL of PK (Proteinase K) used for RNA extraction. Reverse crosslinking occurred via a 65°C incubation overnight. The samples used for immunoblotting were given 10µL of 4X loading buffer before being subject to SDS-PAGE and the immunoblotting method as described above. The RNA samples were resuspended in TRIzol, and total RNA was harvested before the above qPCR protocol was performed.

4.8 *Immunoprecipitation*

After cells were harvested, the samples were subjected to centrifugation at 3000rpm for 3-5 min at 4°C. The pellets were washed with PBS and prepared in lysis buffer (NaCl, 150 mM; Tris, 50 mM; NP-40, 0.5%; dithiothreitol [DTT], 1 mM; and protease inhibitor tablets). After 20 min, lysates were spun down at 10,000rpm for 10 min at 4°C. A Bradford assay then helped determine the biomolecular density of each supernatant. >400μg of total protein were incubated overnight with the respective antibody, followed by protein G-coupled magnetic beads (Life Technologies) for 1 h. FLAG construct co-immunoprecipitation pull downs were instead incubated with anti-FLAG M2 Magnetic Beads (Sigma) overnight or protein G-coupled magnetic beads. Next, the samples were washed thoroughly with lysis buffer. Before immunoprecipitation, beads were treated with RNAse A and t1 for 15 min at room temperature. Finally, samples were resuspended in 4X laemmli loading dye and resolved via SDS-PAGE and visualized via immunoblotting.

4.9 *4SU Labeling*

Following 24 h transfection with either a FLAG-EMPTY or FLAG-SHFL vector, HEK293T cells were pulse labeled with DMEM/FBS containing 500μM 4-Thiouridine (4sU) (Sigma) for 10 min at 37°C. Cells were then washed with PBS before an immediate isolation of total RNA by using TRIzol to harvest the samples. After total RNA was extracted from each sample, 25μg of RNA was subjected to HPDP-biotin treatment, followed by another RNA extraction. Subsequently, Dynabeads MyOne Streptavidin C1 magnetic beads were added to each sample to select for labeled transcripts. All isolated 4sU RNAs were then subjected to RT-qPCR for analysis of the genes of interest. GAPDH was used as the systems' positive control.

4.10 Statistical Analysis

All results in this study are expressed as means ± standard errors of the means (SEMs) of experiments independently repeated at least three times. Unpaired Student's *t* test was used to evaluate the statistical difference between all samples. Significance was evaluated with *P* values as follows: * $p<0.05$; ** $p<0.01$; *** $p<0.001$.

TABLES

Table 1: List of Antibodies used throughout this study.

Antibody	Species	Dilution (IFA)	Dilution (WB)	Source	Cat #
KSHV ORF59	Rabbit	N/A	1:10,000	B. Glaunsinger	N/A
KSHV ORF57	Rabbit	N/A	1:5000	Santa Cruz	sc-135746
KSHV K8.1	Rabbit	N/A	1:10,000	B. Glaunsinger	N/A
KSHV ORF50	Rabbit	N/A	1:5000	B. Glaunsinger	N/A
mCherry	Rabbit	1:100	1:2000	Fisher	PA5-34974
Vinculin	Rabbit	N/A	1:1000	Fisher	700062
DYKDDDDK (FLAG)	Mouse	1:100	1:1000	Fisher	MA1-91878
C19ORF66 (SHFL)	Rabbit	N/A	1:1000	Abcam	ab122765
PABPC	Rabbit	N/A	1:1000	Fisher	PA566900
DDX6	Rabbit	1:100	1:1000	Sigma	SAB4200837
EDC4	Rabbit	1:100	N/A	Fisher	PA5-30485
G3BP	Mouse	1:100	N/A	Abcam	ab56574
TIA-1	Rabbit	1:100	1:1000	Abcam	ab140595

Table 2: List of Primers used throughout this study.

	Forward	**Reverse**
COX2	CCCTTGGGTGTCAAAGGTAA	GCCCTCGCTTATGATCTGTC
CXCL8	AAATCTGGCAACCCTAGTCTG	GTGAGGTAAGATGGTGGCTAAT
ATF3	CAAGAACGAGAAGCAGCATTTG	TTCTGGAGTCCTCCCATTCT
JUNB	TCTACCACGACGACTCATACA	GGCTCGGTTTCAGGAGTTT

REFERENCES

1. Ballestas, M.E., P.A. Chatis and K.M. Kaye. (1999). Efficient persistence of extrachromosomal KSHV DNA mediated by latency-associated nuclear antigen. *Science*. **284**(5414): p. 641-4. 10.1126/science.284.5414.641.

2. Nakamura, H., M. Lu, Y. Gwack, J. Souvlis, S.L. Zeichner, and J.U. Jung. (2003). Global changes in Kaposi's sarcoma-associated virus gene expression patterns following expression of a tetracycline-inducible Rta transactivator. *J Virol*. **77**(7): p. 4205-20. 10.1128/jvi.77.7.4205-4220.2003.

3. Chen, J., K. Ueda, S. Sakakibara, T. Okuno, and K. Yamanishi. (2000). Transcriptional regulation of the Kaposi's sarcoma-associated herpesvirus viral interferon regulatory factor gene. *J Virol*. **74**(18): p. 8623-34. 10.1128/jvi.74.18.8623-8634.2000.

4. Deng, H., A. Young and R. Sun. (2000). Auto-activation of the rta gene of human herpesvirus-8/Kaposi's sarcoma-associated herpesvirus. *J Gen Virol*. **81**(Pt 12): p. 3043-3048. 10.1099/0022-1317-81-12-3043.

5. Duan, W., S. Wang, S. Liu and C. Wood. (2001). Characterization of Kaposi's sarcoma-associated herpesvirus/human herpesvirus-8 ORF57 promoter. *Arch Virol*. **146**(2): p. 403-13. 10.1007/s007050170185.

6. Jeong, J., J. Papin and D. Dittmer. (2001). Differential regulation of the overlapping Kaposi's sarcoma-associated herpesvirus vGCR (orf74) and LANA (orf73) promoters. *J Virol*. **75**(4): p. 1798-807. 10.1128/JVI.75.4.1798-1807.2001.

7. Sakakibara, S., K. Ueda, J. Chen, T. Okuno, and K. Yamanishi. (2001). Octamer-binding sequence is a key element for the autoregulation of Kaposi's sarcoma-associated herpesvirus ORF50/Lyta gene expression. *J Virol*. **75**(15): p. 6894-900. 10.1128/JVI.75.15.6894-6900.2001.

8. Song, M.J., X. Li, H.J. Brown and R. Sun. (2002). Characterization of interactions between RTA and the promoter of polyadenylated nuclear RNA in Kaposi's sarcoma-associated herpesvirus/human herpesvirus 8. *J Virol*. **76**(10): p. 5000-13. 10.1128/jvi.76.10.5000-5013.2002.

9. Zhong, W. and D. Ganem. (1997). Characterization of ribonucleoprotein complexes containing an abundant polyadenylated nuclear RNA encoded by Kaposi's sarcoma-associated herpesvirus (human herpesvirus 8). *J Virol*. **71**(2): p. 1207-12. 10.1128/JVI.71.2.1207-1212.1997.

10. Aneja, K.K. and Y. Yuan. (2017). Reactivation and Lytic Replication of Kaposi's Sarcoma-Associated Herpesvirus: An Update. *Front Microbiol*. **8**: p. 613. 10.3389/fmicb.2017.00613.

11. Covarrubias, S., J.M. Richner, K. Clyde, Y.J. Lee, and B.A. Glaunsinger. (2009). Host shutoff is a conserved phenotype of gammaherpesvirus infection and is orchestrated exclusively from the cytoplasm. *J Virol*. **83**(18): p. 9554-66. 10.1128/JVI.01051-09.

12. Glaunsinger, B. and D. Ganem. (2004). Lytic KSHV infection inhibits host gene expression by accelerating global mRNA turnover. *Mol Cell*. **13**(5): p. 713-23. 10.1016/s1097-2765(04)00091-7.

13. Glaunsinger, B.A. and D.E. Ganem. (2006). Messenger RNA turnover and its regulation in herpesviral infection. *Adv Virus Res*. **66**: p. 337-94. 10.1016/S0065-3527(06)66007-7.

14. Rowe, M., B. Glaunsinger, D. van Leeuwen, J. Zuo, D. Sweetman, D. Ganem., et al. (2007). Host shutoff during productive Epstein-Barr virus infection is mediated by BGLF5 and may contribute to immune evasion. *Proc Natl Acad Sci U S A*. **104**(9): p. 3366-71. 10.1073/pnas.0611128104.

15. Abernathy, E. and B. Glaunsinger. (2015). Emerging roles for RNA degradation in viral replication and antiviral defense. *Virology*. **479-480**: p. 600-8. 10.1016/j.virol.2015.02.007.

16. Gaglia, M.M. and B.A. Glaunsinger. (2010). Viruses and the cellular RNA decay machinery. *Wiley Interdiscip Rev RNA*. **1**(1): p. 47-59. 10.1002/wrna.3.

17. Rivas, H.G., S.K. Schmaling and M.M. Gaglia. (2016). Shutoff of Host Gene Expression in Influenza A Virus and Herpesviruses: Similar Mechanisms and Common Themes. *Viruses*. **8**(4): p. 102. 10.3390/v8040102.

18. Abernathy, E., K. Clyde, R. Yeasmin, L.T. Krug, A. Burlingame, L. Coscoy., et al. (2014). Gammaherpesviral gene expression and virion composition are broadly controlled by accelerated mRNA degradation. *PLoS Pathog*. **10**(1): p. e1003882. 10.1371/journal.ppat.1003882.

19. Richner, J.M., K. Clyde, A.C. Pezda, B.Y. Cheng, T. Wang, G.R. Kumar., et al. (2011). Global mRNA degradation during lytic gammaherpesvirus infection contributes to establishment of viral latency. *PLoS Pathog*. **7**(7): p. e1002150. 10.1371/journal.ppat.1002150.

20. Glaunsinger, B. and D. Ganem. (2004). Highly selective escape from KSHV-mediated host mRNA shutoff and its implications for viral pathogenesis. *J Exp Med*. **200**(3): p. 391-8. 10.1084/jem.20031881.

21. Rodriguez, W., K. Srivastav and M. Muller. (2019). C19ORF66 Broadly Escapes Virus-Induced Endonuclease Cleavage and Restricts Kaposi's Sarcoma-Associated Herpesvirus. *J Virol*. **93**(12)10.1128/JVI.00373-19.

22. Muller, M. and B.A. Glaunsinger. (2017). Nuclease escape elements protect messenger RNA against cleavage by multiple viral endonucleases. *PLoS Pathog*. **13**(8): p. e1006593. 10.1371/journal.ppat.1006593.

23. Abernathy, E., S. Gilbertson, R. Alla and B. Glaunsinger. (2015). Viral Nucleases Induce an mRNA Degradation-Transcription Feedback Loop in Mammalian Cells. *Cell Host Microbe*. **18**(2): p. 243-53. 10.1016/j.chom.2015.06.019.

24. Clyde, K. and B.A. Glaunsinger. (2010). Getting the message direct manipulation of host mRNA accumulation during gammaherpesvirus lytic infection. *Adv Virus Res*. **78**: p. 1-42. 10.1016/B978-0-12-385032-4.00001-X.

25. Clyde, K. and B.A. Glaunsinger. (2011). Deep sequencing reveals direct targets of gammaherpesvirus-induced mRNA decay and suggests that multiple mechanisms govern cellular transcript escape. *PLoS One*. **6**(5): p. e19655. 10.1371/journal.pone.0019655.

26. Hutin, S., Y. Lee and B.A. Glaunsinger. (2013). An RNA element in human interleukin 6 confers escape from degradation by the gammaherpesvirus SOX protein. *J Virol*. **87**(8): p. 4672-82. 10.1128/JVI.00159-13.

27. Lee, Y.J. and B.A. Glaunsinger. (2009). Aberrant herpesvirus-induced polyadenylation correlates with cellular messenger RNA destruction. *PLoS Biol*. **7**(5): p. e1000107. 10.1371/journal.pbio.1000107.

28. Muller, M., S. Hutin, O. Marigold, K.H. Li, A. Burlingame, and B.A. Glaunsinger. (2015). A ribonucleoprotein complex protects the interleukin-6 mRNA from degradation by distinct herpesviral endonucleases. *PLoS Pathog*. **11**(5): p. e1004899. 10.1371/journal.ppat.1004899.

29. Wang, X., Y. Xuan, Y. Han, X. Ding, K. Ye, F. Yang., et al. (2019). Regulation of HIV-1 Gag-Pol Expression by Shiftless, an Inhibitor of Programmed -1 Ribosomal Frameshifting. *Cell*. **176**(3): p. 625-635 e14. 10.1016/j.cell.2018.12.030.

30. Bull, T.M., C.A. Meadows, C.D. Coldren, M. Moore, S.M. Sotto-Santiago, S.P. Nana-Sinkam., et al. (2008). Human herpesvirus-8 infection of primary pulmonary microvascular endothelial cells. *Am J Respir Cell Mol Biol*. **39**(6): p. 706-16. 10.1165/rcmb.2007-0368OC.

31. Gaucher, D., R. Therrien, N. Kettaf, B.R. Angermann, G. Boucher, A. Filali-Mouhim., et al. (2008). Yellow fever vaccine induces integrated multilineage and polyfunctional immune responses. *J Exp Med*. **205**(13): p. 3119-31. 10.1084/jem.20082292.

32. Harvey, S.A., E.G. Romanowski, K.A. Yates and Y.J. Gordon. (2005). Adenovirus-directed ocular innate immunity: the role of conjunctival defensin-like chemokines (IP-10, I-TAC) and phagocytic human defensin-alpha. *Invest Ophthalmol Vis Sci*. **46**(10): p. 3657-65. 10.1167/iovs.05-0438.

33. Kash, J.C., E. Muhlberger, V. Carter, M. Grosch, O. Perwitasari, S.C. Proll., et al. (2006). Global suppression of the host antiviral response by Ebola- and Marburgviruses: increased antagonism of the type I interferon response is associated with enhanced virulence. *J Virol*. **80**(6): p. 3009-20. 10.1128/JVI.80.6.3009-3020.2006.

34. Miyazaki, D., T. Haruki, S. Takeda, S. Sasaki, K. Yakura, Y. Terasaka., et al. (2011). Herpes simplex virus type 1-induced transcriptional networks of corneal endothelial cells indicate antigen presentation function. *Invest Ophthalmol Vis Sci*. **52**(7): p. 4282-93. 10.1167/iovs.10-6911.

35. Wang, J., M.P. Nikrad, T. Phang, B. Gao, T. Alford, Y. Ito., et al. (2011). Innate immune response to influenza A virus in differentiated human alveolar type II cells. *Am J Respir Cell Mol Biol*. **45**(3): p. 582-91. 10.1165/rcmb.2010-0108OC.

36. Xiong, W.C., D.; Irudayam, J.I.; Ali, A.; Yang, O.O.; Arumugaswami, V. (2016). C19ORF66 is an interferon-stimulated gene (ISG) which Inhibits human immunodeficiency virus-1. *BioRxiv*. 10.1101/050310.

37. Zapata, J.C., R. Carrion, Jr., J.L. Patterson, O. Crasta, Y. Zhang, S. Mani., et al. (2013). Transcriptome analysis of human peripheral blood mononuclear cells exposed to Lassa virus and to the attenuated Mopeia/Lassa reassortant 29 (ML29), a vaccine candidate. *PLoS Negl Trop Dis*. **7**(9): p. e2406. 10.1371/journal.pntd.0002406.

38. Balinsky, C.A., H. Schmeisser, A.I. Wells, S. Ganesan, T. Jin, K. Singh., et al. (2017). IRAV (FLJ11286), an Interferon-Stimulated Gene with Antiviral Activity against Dengue Virus, Interacts with MOV10. *J Virol*. **91**(5)10.1128/JVI.01606-16.

39. Hanners, N.W., K.B. Mar, I.N. Boys, J.L. Eitson, P.C. De La Cruz-Rivera, R.B. Richardson., et al. (2021). Shiftless inhibits flavivirus replication in vitro and is neuroprotective in a mouse model of Zika virus pathogenesis. *Proc Natl Acad Sci U S A*. **118**(49)10.1073/pnas.2111266118.

40. Kinast, V., A. Plociennikowska, Anggakusuma, T. Bracht, D. Todt, R.J.P. Brown., et al. (2020). C19orf66 is an interferon-induced inhibitor of HCV replication that restricts formation of the viral replication organelle. *J Hepatol*. **73**(3): p. 549-558. 10.1016/j.jhep.2020.03.047.

41. Napthine, S., C.H. Hill, H.C.M. Nugent and I. Brierley. (2021). Modulation of Viral Programmed Ribosomal Frameshifting and Stop Codon Readthrough by the Host Restriction Factor Shiftless. *Viruses*. **13**(7)10.3390/v13071230.

42. Rodriguez, W., T. Mehrmann, D. Hatfield and M. Muller. (2022). Shiftless Restricts Viral Gene Expression and Influences RNA Granule Formation during Kaposi's Sarcoma-Associated Herpesvirus Lytic Replication. *J Virol*. **96**(22): p. e0146922. 10.1128/jvi.01469-22.

43. Suzuki, Y., W.X. Chin, Q. Han, K. Ichiyama, C.H. Lee, Z.W. Eyo., et al. (2016). Characterization of RyDEN (C19orf66) as an Interferon-Stimulated Cellular Inhibitor against Dengue Virus Replication. *PLoS Pathog*. **12**(1): p. e1005357. 10.1371/journal.ppat.1005357.

44. Wang, H., N. Kong, Y. Jiao, S. Dong, D. Sun, X. Chen., et al. (2021). EGR1 Suppresses Porcine Epidemic Diarrhea Virus Replication by Regulating IRAV To Degrade Viral Nucleocapsid Protein. *J Virol*. **95**(19): p. e0064521. 10.1128/JVI.00645-21.

45. Wu, Y., X. Yang, Z. Yao, X. Dong, D. Zhang, Y. Hu., et al. (2020). C19orf66 interrupts Zika virus replication by inducing lysosomal degradation of viral NS3. *PLoS Negl Trop Dis*. **14**(3): p. e0008083. 10.1371/journal.pntd.0008083.

46. Yu, D., Y. Zhao, J. Pan, X. Yang, Z. Liang, S. Xie., et al. (2021). C19orf66 Inhibits Japanese Encephalitis Virus Replication by Targeting -1 PRF and the NS3 Protein. *Virol Sin*. **36**(6): p. 1443-1455. 10.1007/s12250-021-00423-6.

47. Benner, B.E., J.W. Bruce, J.R. Kentala, M. Murray, J.T. Becker, P. Garcia-Miranda., et al. (2022). Perturbing HIV-1 Ribosomal Frameshifting Frequency Reveals a cis Preference for Gag-Pol Incorporation into Assembling Virions. *J Virol*. **96**(1): p. e0134921. 10.1128/JVI.01349-21.

48. Halma, M.T.J., D.B. Ritchie, T.R. Cappellano, K. Neupane, and M.T. Woodside. (2019). Complex dynamics under tension in a high-efficiency frameshift stimulatory structure. *Proc Natl Acad Sci U S A*. **116**(39): p. 19500-19505. 10.1073/pnas.1905258116.

49. Zhou, D., F. Jia, Q. Li, L. Zhang, Z. Chen, Z. Zhao., et al. (2018). Japanese Encephalitis Virus NS1' Protein Antagonizes Interferon Beta Production. *Virol Sin*. **33**(6): p. 515-523. 10.1007/s12250-018-0067-5.

50. Zimmer, M.M., A. Kibe, U. Rand, L. Pekarek, L. Ye, S. Buck., et al. (2021). The short isoform of the host antiviral protein ZAP acts as an inhibitor of SARS-CoV-2 programmed ribosomal frameshifting. *Nat Commun*. **12**(1): p. 7193. 10.1038/s41467-021-27431-0.

51. Ritchie, D.B., T.R. Cappellano, C. Tittle, N. Rezajooei, L. Rouleau, W.K.A. Sikkema., et al. (2017). Conformational dynamics of the frameshift stimulatory structure in HIV-1. *RNA*. **23**(9): p. 1376-1384. 10.1261/rna.061655.117.

52. Chiabudini, M., A. Tais, Y. Zhang, S. Hayashi, T. Wolfle, E. Fitzke., et al. (2014). Release factor eRF3 mediates premature translation termination on polylysine-stalled ribosomes in Saccharomyces cerevisiae. *Mol Cell Biol*. **34**(21): p. 4062-76. 10.1128/MCB.00799-14.

53. Rodriguez, W. and M. Muller. (2022). Shiftless, a Critical Piece of the Innate Immune Response to Viral Infection. *Viruses*. **14**(6)10.3390/v14061338.

54. Kenny, P.J., M. Kim, G. Skariah, J. Nielsen, M.C. Lannom, and S. Ceman. (2020). The FMRP-MOV10 complex: a translational regulatory switch modulated by G-Quadruplexes. *Nucleic Acids Res*. **48**(2): p. 862-878. 10.1093/nar/gkz1092.

55. Pabis, M., G.M. Popowicz, R. Stehle, D. Fernandez-Ramos, S. Asami, L. Warner., et al. (2019). HuR biological function involves RRM3-mediated dimerization and RNA binding by all three RRMs. *Nucleic Acids Res*. **47**(2): p. 1011-1029. 10.1093/nar/gky1138.

56. Park, Y., J. Park, H.J. Hwang, B. Kim, K. Jeong, J. Chang., et al. (2020). Nonsense-mediated mRNA decay factor UPF1 promotes aggresome formation. *Nat Commun*. **11**(1): p. 3106. 10.1038/s41467-020-16939-6.

57. Qi, Y., M. Wang and Q. Jiang. (2022). PABPC1--mRNA stability, protein translation and tumorigenesis. *Front Oncol*. **12**: p. 1025291. 10.3389/fonc.2022.1025291.

58. Brook, M. and N.K. Gray. (2012). The role of mammalian poly(A)-binding proteins in co-ordinating mRNA turnover. *Biochem Soc Trans*. **40**(4): p. 856-64. 10.1042/BST20120100.

59. Burgess, H.M. and N.K. Gray. (2010). mRNA-specific regulation of translation by poly(A)-binding proteins. *Biochem Soc Trans*. **38**(6): p. 1517-22. 10.1042/BST0381517.

60. Fabbri, L., A. Chakraborty, C. Robert and S. Vagner. (2021). The plasticity of mRNA translation during cancer progression and therapy resistance. *Nat Rev Cancer*. **21**(9): p. 558-577. 10.1038/s41568-021-00380-y.

61. Goss, D.J. and F.E. Kleiman. (2013). Poly(A) binding proteins: are they all created equal? *Wiley Interdiscip Rev RNA*. **4**(2): p. 167-79. 10.1002/wrna.1151.

62. Hosoda, N., F. Lejeune and L.E. Maquat. (2006). Evidence that poly(A) binding protein C1 binds nuclear pre-mRNA poly(A) tails. *Mol Cell Biol*. **26**(8): p. 3085-97. 10.1128/MCB.26.8.3085-3097.2006.

63. Kuhn, U. and E. Wahle. (2004). Structure and function of poly(A) binding proteins. *Biochim Biophys Acta*. **1678**(2-3): p. 67-84. 10.1016/j.bbaexp.2004.03.008.

64. Smith, R.W., T.K. Blee and N.K. Gray. (2014). Poly(A)-binding proteins are required for diverse biological processes in metazoans. *Biochem Soc Trans*. **42**(4): p. 1229-37. 10.1042/BST20140111.

65. Polacek, C., P. Friebe and E. Harris. (2009). Poly(A)-binding protein binds to the non-polyadenylated 3' untranslated region of dengue virus and modulates translation efficiency. *J Gen Virol*. **90**(Pt 3): p. 687-692. 10.1099/vir.0.007021-0.

66. Burrows, C., N. Abd Latip, S.J. Lam, L. Carpenter, K. Sawicka, G. Tzolovsky., et al. (2010). The RNA binding protein Larp1 regulates cell division, apoptosis and cell migration. *Nucleic Acids Res*. **38**(16): p. 5542-53. 10.1093/nar/gkq294.

67. Dantas, G., A.L. Watters, B.M. Lunde, Z.M. Eletr, N.G. Isern, T. Roseman., et al. (2006). Mis-translation of a computationally designed protein yields an exceptionally stable homodimer: implications for protein engineering and evolution. *J Mol Biol*. **362**(5): p. 1004-24. 10.1016/j.jmb.2006.07.092.

68. Franco, R., A. Cordomi, C. Llinas Del Torrent, A. Lillo, J. Serrano-Marin, G. Navarro., et al. (2021). Structure and function of adenosine receptor heteromers. *Cell Mol Life Sci*. **78**(8): p. 3957-3968. 10.1007/s00018-021-03761-6.

69. Majerciak, V. and Z.M. Zheng. (2015). KSHV ORF57, a protein of many faces. *Viruses*. **7**(2): p. 604-33. 10.3390/v7020604.

70. Taylor, A., B.R. Jackson, M. Noerenberg, D.J. Hughes, J.R. Boyne, M. Verow., et al. (2011). Mutation of a C-terminal motif affects Kaposi's sarcoma-associated herpesvirus ORF57 RNA binding, nuclear trafficking, and multimerization. *J Virol*. **85**(15): p. 7881-91. 10.1128/JVI.00138-11.

71. Banani, S.F., H.O. Lee, A.A. Hyman and M.K. Rosen. (2017). Biomolecular condensates: organizers of cellular biochemistry. *Nat Rev Mol Cell Biol*. **18**(5): p. 285-298. 10.1038/nrm.2017.7.

72. Dundr, M., M.D. Hebert, T.S. Karpova, D. Stanek, H. Xu, K.B. Shpargel., et al. (2004). In vivo kinetics of Cajal body components. *J Cell Biol*. **164**(6): p. 831-42. 10.1083/jcb.200311121.

73. Phair, R.D. and T. Misteli. (2000). High mobility of proteins in the mammalian cell nucleus. *Nature*. **404**(6778): p. 604-9. 10.1038/35007077.

74. Weidtkamp-Peters, S., T. Lenser, D. Negorev, N. Gerstner, T.G. Hofmann, G. Schwanitz., et al. (2008). Dynamics of component exchange at PML nuclear bodies. *J Cell Sci*. **121**(Pt 16): p. 2731-43. 10.1242/jcs.031922.

75. Hirose, T., K. Ninomiya, S. Nakagawa and T. Yamazaki. (2023). A guide to membraneless organelles and their various roles in gene regulation. *Nat Rev Mol Cell Biol*. **24**(4): p. 288-304. 10.1038/s41580-022-00558-8.

76. Ivanov, P., N. Kedersha and P. Anderson. (2019). Stress Granules and Processing Bodies in Translational Control. *Cold Spring Harb Perspect Biol*. **11**(5)10.1101/cshperspect.a032813.

77. Millar, S.R., J.Q. Huang, K.J. Schreiber, Y.C. Tsai, J. Won, J. Zhang., et al. (2023). A New Phase of Networking: The Molecular Composition and Regulatory Dynamics of Mammalian Stress Granules. *Chem Rev*. **123**(14): p. 9036-9064. 10.1021/acs.chemrev.2c00608.

78. Mittag, T. and R.V. Pappu. (2022). A conceptual framework for understanding phase separation and addressing open questions and challenges. *Mol Cell*. **82**(12): p. 2201-2214. 10.1016/j.molcel.2022.05.018.

79. Audas, T.E., D.E. Audas, M.D. Jacob, J.J. Ho, M. Khacho, M. Wang., et al. (2016). Adaptation to Stressors by Systemic Protein Amyloidogenesis. *Dev Cell*. **39**(2): p. 155-168. 10.1016/j.devcel.2016.09.002.

80. Biamonti, G. and C. Vourc'h. (2010). Nuclear stress bodies. *Cold Spring Harb Perspect Biol*. **2**(6): p. a000695. 10.1101/cshperspect.a000695.

81. Ninomiya, K., J. Iwakiri, M.K. Aly, Y. Sakaguchi, S. Adachi, T. Natsume., et al. (2021). m(6) A modification of HSATIII lncRNAs regulates temperature-dependent splicing. *EMBO J*. **40**(15): p. e107976. 10.15252/embj.2021107976.

82. Andrei, M.A., D. Ingelfinger, R. Heintzmann, T. Achsel, R. Rivera-Pomar, and R. Luhrmann. (2005). A role for eIF4E and eIF4E-transporter in targeting mRNPs to mammalian processing bodies. *RNA*. **11**(5): p. 717-27. 10.1261/rna.2340405.

83. Bashkirov, V.I., H. Scherthan, J.A. Solinger, J.M. Buerstedde, and W.D. Heyer. (1997). A mouse cytoplasmic exoribonuclease (mXRN1p) with preference for G4 tetraplex substrates. *J Cell Biol*. **136**(4): p. 761-73. 10.1083/jcb.136.4.761.

84. Sheth, U. and R. Parker. (2003). Decapping and decay of messenger RNA occur in cytoplasmic processing bodies. *Science*. **300**(5620): p. 805-8. 10.1126/science.1082320.

85. Brengues, M., D. Teixeira and R. Parker. (2005). Movement of eukaryotic mRNAs between polysomes and cytoplasmic processing bodies. *Science*. **310**(5747): p. 486-9. 10.1126/science.1115791.

86. Eulalio, A., I. Behm-Ansmant, D. Schweizer and E. Izaurralde. (2007). P-body formation is a consequence, not the cause, of RNA-mediated gene silencing. *Mol Cell Biol*. **27**(11): p. 3970-81. 10.1128/MCB.00128-07.

87. Pitchiaya, S., M.D.A. Mourao, A.P. Jalihal, L. Xiao, X. Jiang, A.M. Chinnaiyan., et al. (2019). Dynamic Recruitment of Single RNAs to Processing Bodies Depends on RNA Functionality. *Mol Cell*. **74**(3): p. 521-533 e6. 10.1016/j.molcel.2019.03.001.

88. Kedersha, N., M.R. Cho, W. Li, P.W. Yacono, S. Chen, N. Gilks., et al. (2000). Dynamic shuttling of TIA-1 accompanies the recruitment of mRNA to mammalian stress granules. *J Cell Biol*. **151**(6): p. 1257-68. 10.1083/jcb.151.6.1257.

89. Kedersha, N., G. Stoecklin, M. Ayodele, P. Yacono, J. Lykke-Andersen, M.J. Fritzler., et al. (2005). Stress granules and processing bodies are dynamically linked sites of mRNP remodeling. *J Cell Biol*. **169**(6): p. 871-84. 10.1083/jcb.200502088.

90. Kedersha, N. and P. Anderson. (2007). Mammalian stress granules and processing bodies. *Methods Enzymol*. **431**: p. 61-81. 10.1016/S0076-6879(07)31005-7.

91. Fujimura, K., T. Suzuki, Y. Yasuda, M. Murata, J. Katahira, and Y. Yoneda. (2010). Identification of importin alpha1 as a novel constituent of RNA stress granules. *Biochim Biophys Acta*. **1803**(7): p. 865-71. 10.1016/j.bbamcr.2010.03.020.

92. Fukuda, T., T. Naiki, M. Saito and K. Irie. (2009). hnRNP K interacts with RNA binding motif protein 42 and functions in the maintenance of cellular ATP level during stress conditions. *Genes Cells*. **14**(2): p. 113-28. 10.1111/j.1365-2443.2008.01256.x.

93. Valentin-Vega, Y.A., Y.D. Wang, M. Parker, D.M. Patmore, A. Kanagaraj, J. Moore., et al. (2016). Cancer-associated DDX3X mutations drive stress granule assembly and impair global translation. *Sci Rep*. **6**: p. 25996. 10.1038/srep25996.

94. Yasuda, K., H. Zhang, D. Loiselle, T. Haystead, I.G. Macara, and S. Mili. (2013). The RNA-binding protein Fus directs translation of localized mRNAs in APC-RNP granules. *J Cell Biol*. **203**(5): p. 737-46. 10.1083/jcb.201306058.

95. Anderson, P., N. Kedersha and P. Ivanov. (2015). Stress granules, P-bodies and cancer. *Biochim Biophys Acta*. **1849**(7): p. 861-70. 10.1016/j.bbagrm.2014.11.009.

96. Corbet, G.A. and R. Parker. (2019). RNP Granule Formation: Lessons from P-Bodies and Stress Granules. *Cold Spring Harb Symp Quant Biol*. **84**: p. 203-215. 10.1101/sqb.2019.84.040329.

97. Fan, A.C. and A.K. Leung. (2016). RNA Granules and Diseases: A Case Study of Stress Granules in ALS and FTLD. *Adv Exp Med Biol*. **907**: p. 263-96. 10.1007/978-3-319-29073-7_11.

98. Guzikowski, A.R., Y.S. Chen and B.M. Zid. (2019). Stress-induced mRNP granules: Form and function of processing bodies and stress granules. *Wiley Interdiscip Rev RNA*. **10**(3): p. e1524. 10.1002/wrna.1524.

99. Riggs, C.L., N. Kedersha, P. Ivanov and P. Anderson. (2020). Mammalian stress granules and P bodies at a glance. *J Cell Sci*. **133**(16)10.1242/jcs.242487.

100. Tauber, D., G. Tauber and R. Parker. (2020). Mechanisms and Regulation of RNA Condensation in RNP Granule Formation. *Trends Biochem Sci*. **45**(9): p. 764-778. 10.1016/j.tibs.2020.05.002.

101. Tian, S., H.A. Curnutte and T. Trcek. (2020). RNA Granules: A View from the RNA Perspective. *Molecules*. **25**(14)10.3390/molecules25143130.

102. Reineke, L.C. and R.E. Lloyd. (2013). Diversion of stress granules and P-bodies during viral infection. *Virology*. **436**(2): p. 255-67. 10.1016/j.virol.2012.11.017.

103. Corcoran, J.A., B.P. Johnston and C. McCormick. (2015). Viral activation of MK2-hsp27-p115RhoGEF-RhoA signaling axis causes cytoskeletal rearrangements, p-body disruption and ARE-mRNA stabilization. *PLoS Pathog*. **11**(1): p. e1004597. 10.1371/journal.ppat.1004597.

104. Sharma, N.R., V. Majerciak, M.J. Kruhlak, L. Yu, J.G. Kang, A. Yang., et al. (2019). KSHV RNA-binding protein ORF57 inhibits P-body formation to promote viral multiplication by interaction with Ago2 and GW182. *Nucleic Acids Res*. **47**(17): p. 9368-9385. 10.1093/nar/gkz683.

105. Robinson, C.A., G.K. Singh, M. Kleer, T. Katsademas, E.L. Castle, B.Q. Boudreau., et al. (2023). Kaposi's sarcoma-associated herpesvirus (KSHV) utilizes the NDP52/CALCOCO2 selective autophagy receptor to disassemble processing bodies. *PLoS Pathog*. **19**(1): p. e1011080. 10.1371/journal.ppat.1011080.

106. Ariumi, Y., M. Kuroki, K. Abe, H. Dansako, M. Ikeda, T. Wakita., et al. (2007). DDX3 DEAD-box RNA helicase is required for hepatitis C virus RNA replication. *J Virol*. **81**(24): p. 13922-6. 10.1128/JVI.01517-07.

107. Ariumi, Y., M. Kuroki, Y. Kushima, K. Osugi, M. Hijikata, M. Maki., et al. (2011). Hepatitis C virus hijacks P-body and stress granule components around lipid droplets. *J Virol*. **85**(14): p. 6882-92. 10.1128/JVI.02418-10.

108. Chahar, H.S., S. Chen and N. Manjunath. (2013). P-body components LSM1, GW182, DDX3, DDX6 and XRN1 are recruited to WNV replication sites and positively regulate viral replication. *Virology*. **436**(1): p. 1-7. 10.1016/j.virol.2012.09.041.

109. Jangra, R.K., M. Yi and S.M. Lemon. (2010). DDX6 (Rck/p54) is required for efficient hepatitis C virus replication but not for internal ribosome entry site-directed translation. *J Virol*. **84**(13): p. 6810-24. 10.1128/JVI.00397-10.

110. Pager, C.T., S. Schutz, T.M. Abraham, G. Luo, and P. Sarnow. (2013). Modulation of hepatitis C virus RNA abundance and virus release by dispersion of processing bodies and enrichment of stress granules. *Virology*. **435**(2): p. 472-84. 10.1016/j.virol.2012.10.027.

111. Perez-Vilaro, G., N. Scheller, V. Saludes and J. Diez. (2012). Hepatitis C virus infection alters P-body composition but is independent of P-body granules. *J Virol*. **86**(16): p. 8740-9. 10.1128/JVI.07167-11.

112. Scheller, N., L.B. Mina, R.P. Galao, A. Chari, M. Gimenez-Barcons, A. Noueiry., et al. (2009). Translation and replication of hepatitis C virus genomic RNA depends on ancient cellular proteins that control mRNA fates. *Proc Natl Acad Sci U S A*. **106**(32): p. 13517-22. 10.1073/pnas.0906413106.

113. Bol, G.M., M. Xie and V. Raman. (2015). DDX3, a potential target for cancer treatment. *Mol Cancer*. **14**: p. 188. 10.1186/s12943-015-0461-7.

114. Chao, C.H., C.M. Chen, P.L. Cheng, J.W. Shih, A.P. Tsou, and Y.H. Lee. (2006). DDX3, a DEAD box RNA helicase with tumor growth-suppressive property and transcriptional regulation activity of the p21waf1/cip1 promoter, is a candidate tumor suppressor. *Cancer Res*. **66**(13): p. 6579-88. 10.1158/0008-5472.CAN-05-2415.

115. Geissler, R., R.P. Golbik and S.E. Behrens. (2012). The DEAD-box helicase DDX3 supports the assembly of functional 80S ribosomes. *Nucleic Acids Res*. **40**(11): p. 4998-5011. 10.1093/nar/gks070.

116. Jankowsky, A., U.P. Guenther and E. Jankowsky. (2011). The RNA helicase database. *Nucleic Acids Res*. **39**(Database issue): p. D338-41. 10.1093/nar/gkq1002.

117. Lai, M.C., Y.H. Lee and W.Y. Tarn. (2008). The DEAD-box RNA helicase DDX3 associates with export messenger ribonucleoproteins as well as tip-associated protein and participates in translational control. *Mol Biol Cell*. **19**(9): p. 3847-58. 10.1091/mbc.e07-12-1264.

118. Lee, C.S., A.P. Dias, M. Jedrychowski, A.H. Patel, J.L. Hsu, and R. Reed. (2008). Human DDX3 functions in translation and interacts with the translation initiation factor eIF3. *Nucleic Acids Res*. **36**(14): p. 4708-18. 10.1093/nar/gkn454.

119. Linder, P. and E. Jankowsky. (2011). From unwinding to clamping - the DEAD box RNA helicase family. *Nat Rev Mol Cell Biol*. **12**(8): p. 505-16. 10.1038/nrm3154.

120. Merz, C., H. Urlaub, C.L. Will and R. Luhrmann. (2007). Protein composition of human mRNPs spliced in vitro and differential requirements for mRNP protein recruitment. *RNA*. **13**(1): p. 116-28. 10.1261/rna.336807.

121. Schroder, M. (2011). Viruses and the human DEAD-box helicase DDX3: inhibition or exploitation? *Biochem Soc Trans*. **39**(2): p. 679-83. 10.1042/BST0390679.

122. Shih, J.W., T.Y. Tsai, C.H. Chao and Y.H. Wu Lee. (2008). Candidate tumor suppressor DDX3 RNA helicase specifically represses cap-dependent translation by acting as an eIF4E inhibitory protein. *Oncogene*. **27**(5): p. 700-14. 10.1038/sj.onc.1210687.

123. Soto-Rifo, R. and T. Ohlmann. (2013). The role of the DEAD-box RNA helicase DDX3 in mRNA metabolism. *Wiley Interdiscip Rev RNA*. **4**(4): p. 369-85. 10.1002/wrna.1165.

124. Soto-Rifo, R., P.S. Rubilar, T. Limousin, S. de Breyne, D. Decimo, and T. Ohlmann. (2012). DEAD-box protein DDX3 associates with eIF4F to promote translation of selected mRNAs. *EMBO J*. **31**(18): p. 3745-56. 10.1038/emboj.2012.220.

125. Mo, J., H. Liang, C. Su, P. Li, J. Chen, and B. Zhang. (2021). DDX3X: structure, physiologic functions and cancer. *Mol Cancer*. **20**(1): p. 38. 10.1186/s12943-021-01325-7.

126. Chen, H.H., H.I. Yu, W.C. Cho and W.Y. Tarn. (2015). DDX3 modulates cell adhesion and motility and cancer cell metastasis via Rac1-mediated signaling pathway. *Oncogene*. **34**(21): p. 2790-800. 10.1038/onc.2014.190.

127. Lai, M.C., W.C. Chang, S.Y. Shieh and W.Y. Tarn. (2010). DDX3 regulates cell growth through translational control of cyclin E1. *Mol Cell Biol*. **30**(22): p. 5444-53. 10.1128/MCB.00560-10.

128. Chang, P.C., C.W. Chi, G.Y. Chau, F.Y. Li, Y.H. Tsai, J.C. Wu., et al. (2006). DDX3, a DEAD box RNA helicase, is deregulated in hepatitis virus-associated hepatocellular carcinoma and is involved in cell growth control. *Oncogene*. **25**(14): p. 1991-2003. 10.1038/sj.onc.1209239.

129. Kellaris, G., K. Khan, S.M. Baig, I.C. Tsai, F.M. Zamora, P. Ruggieri., et al. (2018). A hypomorphic inherited pathogenic variant in DDX3X causes male intellectual disability with additional neurodevelopmental and neurodegenerative features. *Hum Genomics*. **12**(1): p. 11. 10.1186/s40246-018-0141-y.

130. Tantravedi, S., F. Vesuna, P.T. Winnard, Jr., M.R.H. Van Voss, P.J. Van Diest, and V. Raman. (2017). Role of DDX3 in the pathogenesis of inflammatory bowel disease. *Oncotarget*. **8**(70): p. 115280-115289. 10.18632/oncotarget.23323.

131. Blanco, F.F., S. Sanduja, N.G. Deane, P.J. Blackshear, and D.A. Dixon. (2014). Transforming growth factor beta regulates P-body formation through induction of the mRNA decay factor tristetraprolin. *Mol Cell Biol*. **34**(2): p. 180-95. 10.1128/MCB.01020-13.

132. Corcoran, J.A., D.A. Khaperskyy, B.P. Johnston, C.A. King, D.P. Cyr, A.V. Olsthoorn., et al. (2012). Kaposi's sarcoma-associated herpesvirus G-protein-coupled receptor prevents AU-rich-element-mediated mRNA decay. *J Virol*. **86**(16): p. 8859-71. 10.1128/JVI.00597-12.

133. Franks, T.M. and J. Lykke-Andersen. (2007). TTP and BRF proteins nucleate processing body formation to silence mRNAs with AU-rich elements. *Genes Dev*. **21**(6): p. 719-35. 10.1101/gad.1494707.

134. Kleer, M., R.P. Mulloy, C.A. Robinson, D. Evseev, M.P. Bui-Marinos, E.L. Castle., et al. (2022). Human coronaviruses disassemble processing bodies. *PLoS Pathog*. **18**(8): p. e1010724. 10.1371/journal.ppat.1010724.

135. Vindry, C., A. Marnef, H. Broomhead, L. Twyffels, S. Ozgur, G. Stoecklin., et al. (2017). Dual RNA Processing Roles of Pat1b via Cytoplasmic Lsm1-7 and Nuclear Lsm2-8 Complexes. *Cell Rep*. **20**(5): p. 1187-1200. 10.1016/j.celrep.2017.06.091.

136. Yang, W. H., et al. (2006). "RNA-associated protein 55 (RAP55) localizes to mRNA processing bodies and stress granules." *RNA* **12**(4): 547-554.

137. Ayache, J., et al. (2015). "P-body assembly requires DDX6 repression complexes rather than decay or Ataxin2/2L complexes." *Mol Biol Cell* **26**(14): 2579-2595.

138. Ozgur, S., et al. (2010). "Human Pat1b connects deadenylation with mRNA decapping and controls the assembly of processing bodies." *Mol Cell Biol* **30**(17): 4308-4323.

139. Yu, J. H., et al. (2005). "Ge-1 is a central component of the mammalian cytoplasmic mRNA processing body." *RNA* **11**(12): 1795-1802.

140. Na, Z., et al. (2020). "The NBDY Microprotein Regulates Cellular RNA Decapping." *Biochemistry* **59**(42): 4131-4142.

141. Na, Z., et al. (2021). "Phosphorylation of a Human Microprotein Promotes Dissociation of Biomolecular Condensates." *J Am Chem Soc* **143**(32): 12675-12687.

142. Soulier, J., L. Grollet, E. Oksenhendler, P. Cacoub, D. Cazals-Hatem, P. Babinet., et al. (1995). Kaposi's sarcoma-associated herpesvirus-like DNA sequences in multicentric Castleman's disease. *Blood*. **86**(4): p. 1276-80.

143. Cesarman, E., Y. Chang, P.S. Moore, J.W. Said, and D.M. Knowles. (1995). Kaposi's sarcoma-associated herpesvirus-like DNA sequences in AIDS-related body-cavity-based lymphomas. *N Engl J Med*. **332**(18): p. 1186-91. 10.1056/NEJM199505043321802.

144. Sarid, R., S.J. Olsen and P.S. Moore. (1999). Kaposi's sarcoma-associated herpesvirus: epidemiology, virology, and molecular biology. *Adv Virus Res*. **52**: p. 139-232. 10.1016/s0065-3527(08)60299-7.

145. Mathew, S.F., C. Crowe-McAuliffe, R. Graves, T.S. Cardno, C. McKinney, E.S. Poole., et al. (2015). The highly conserved codon following the slippery sequence supports -1 frameshift efficiency at the HIV-1 frameshift site. *PLoS One*. **10**(3): p. e0122176. 10.1371/journal.pone.0122176.

146. Hubstenberger, A., M. Courel, M. Benard, S. Souquere, M. Ernoult-Lange, R. Chouaib., et al. (2017). P-Body Purification Reveals the Condensation of Repressed mRNA Regulons. *Mol Cell*. **68**(1): p. 144-157 e5. 10.1016/j.molcel.2017.09.003.

147. Zheng, D., N. Ezzeddine, C.Y. Chen, W. Zhu, X. He, and A.B. Shyu. (2008). Deadenylation is prerequisite for P-body formation and mRNA decay in mammalian cells. *J Cell Biol*. **182**(1): p. 89-101. 10.1083/jcb.200801196.

148. Brothers, W.R., H. Fakim, S. Kajjo and M.R. Fabian. (2022). P-bodies directly regulate MARF1-mediated mRNA decay in human cells. *Nucleic Acids Res*. **50**(13): p. 7623-7636. 10.1093/nar/gkac557.

The views expressed in this submission are those of the author and do not reflect the official policy or position of the United States Air Force, Department of Defense, or the U.S. Government.